SKB

TECHNICAL REPORT 92-34

Sensitivity study of rock mass response to glaciation at Finnsjön, central Sweden

Jan Israelsson[1], Lars Rosengren[1], Ove Stephansson[2]

[1] Itasca Geomekanik AB, Falun, Sweden
[2] Royal Institute of Technology, Dept. of Engineering Geology, Stockholm, Sweden

November 1992

SVENSK KÄRNBRÄNSLEHANTERING AB
SWEDISH NUCLEAR FUEL AND WASTE MANAGEMENT CO

BOX 5864 S-102 48 STOCKHOLM

TEL 08-665 28 00 TELEX 13108 SKB S
TELEFAX 08-661 57 19

SENSITIVITY STUDY OF ROCK MASS RESPONSE TO GLACIATION AT FINNSJÖN, CENTRAL SWEDEN

Jan Israelsson[1], Lars Rosengren[1], Ove Stephansson[2]

1 Itasca Geomekanik AB, Falun, Sweden
2 Royal Institute of Technology, Dept. of Engineering Geology, Stockholm, Sweden

November 1992

This report concerns a study which was conducted for SKB. The conclusions and viewpoints presented in the report are those of the author(s) and do not necessarily coincide with those of the client.

Information on SKB technical reports from 1977-1978 (TR 121), 1979 (TR 79-28), 1980 (TR 80-26), 1981 (TR 81-17), 1982 (TR 82-28), 1983 (TR 83-77), 1984 (TR 85-01), 1985 (TR 85-20), 1986 (TR 86-31), 1987 (TR 87-33), 1988 (TR 88-32), 1989 (TR 89-40), 1990 (TR 90-46) and 1991 (TR 91-64) is available through SKB.

SENSITIVITY STUDY OF ROCK MASS RESPONSE TO GLACIATION AT FINNSJÖN, CENTRAL SWEDEN

Prepared for:

SKB

Swedish Nuclear Fuel and Waste Management Co.
Box 5864
S-102 48 Stockholm, Sweden

Prepared by:

Jan Israelsson[1]
Lars Rosengren[1]
Ove Stephansson[2]

[1]Itasca Geomekanik AB, Stigaregatan 5, S-791 60 Falun, Sweden
[2]Royal Institute of Technology, Dept. of Engineering Geology,
S-100 44 Stockholm, Sweden

November 1992

Keywords: Rock Mechanics, Glaciation load, Sensitivity study

ABSTRACT

The safety analysis SKB-91 of the Swedish Nuclear Fuel and Waste Management Company (SKB) paid specific attention to the glaciation scenario and related phenomena. In the first phase, Rosengren and Stephansson (1990), used the distinct element computer code UDEC to examine the response of the rock mass in the Finnsjön area to the processes of glaciation and deglaciation.

This report describes the second phase, in which the sensitivity of the results to different in-situ stresses and fault zone strength properties have been analyzed. A statistical approach was used to extrapolate the range of in-situ stresses at depth from measured in-situ stresses at shallower depths. Three different linear in-situ stress variations with depth were defined using a 99% confidence interval. For each in-situ stress case, three fault zone strength assumptions were analyzed for an ice loading sequence, involving 3 km, 1 km, 0-1 km (ice wedge) and 0 km of ice thickness. Each combination of in-situ stress and fault zone strength was analyzed with and without an ice lake, situated on top of the ice sheet. Consequently, a total of 18 models were studied.

The results indicated significant differences in stress distribution, failure (reactivation) of fault zones, and shear displacement on fault zones for some combinations of in-situ stress, fault zone strength, and ice lake pressure. Based on the results, several preliminary recommendations for repository siting are made, as well as recommendations for further study.

ABSTRACT (in Swedish)

I säkerhetsanalysen SKB-91, som utförts av Svensk Kärnbränslehantering AB, (SKB), har uppmärksamhet speciellt ägnats åt glaciation och därtill hörande fenomen. I en första fas studerade Rosengren och Stephansson (1990), med hjälp av det distinkta element-programmet UDEC, hur en glaciationsprocess med istillväxt och avsmältning kan påverka bergmassan i Finnsjö-området.

Denna rapport beskriver fas två, i vilken resultatens känslighet med avseende på ansatt in-situ spänning och hållfasthet i svaghetszoner har analyserats. De uppmätta spänningarna har analyserats statistiskt för att extrapolera uppmätta in-situ spänningar mot djupet. Tre olika linjära ansatser om in-situ spänningarnas variation med djupet togs fram med hjälp av det 99% konfidensintervallet. För var och en av spänningsansatserna studerades tre hållfasthetsnivåer för svaghetszonerna. Belastningssekvensen i analyserna omfattade islaster med tjockleken 3 km, 1 km, 0-1 km (kilformad islast) och 0 km. Varje kombination av in-situ spänningar och svaghetszonernas hållfasthet analyserades med och utan den portrycksökning som en issjö, belägen på glaciärisen, ger upphov till i svaghetszonerna. Sammantaget innebär detta att 18 modeller analyserades.

Resultaten indikerade stora skillnader i spänningsfördelning, hållfasthetsöverskridanden i svaghetszoner med åtföljande reaktivering samt skjuvrörelser längs svaghetszoner beroende på vilken kombination av in-situ spänningar, hållfasthet i svaghetszonerna och portryck från issjö som analyserades. Flera rekommendationer om lokaliceringen av ett lager och fortsatta studier lämnas i rapporten.

SUMMARY

Rosengren and Stephansson (1990) examined the response of the rock mass in the Finnsjön area to the processes of glaciation and deglaciation, including isostatic movement and ice lake water pressure, using the distinct element computer code UDEC.

The study presented in this report, concerns the sensitivity of the Finnsjön rock mass response to variations in i) in-situ state of stress and ii) the strength properties of the fault zones. Results from 18 different combinations of in-situ stress, fault zone strength and pore pressure in the fault zones are presented.

The in-situ stress and fault zone strengths were chosen for sensitivity study for the following reasons:

1. measured in-situ stresses, which are extrapolated down to a depth of 2000 m, are uncertain due to the scattering, and

2. in the previous study, strength parameters of the fault zones were estimated and not based on actual laboratory or field tests.

Three steps of ice loading were simulated. For each loading step, two simulations were conducted: one without and one with an ice lake situated on top of the ice sheet. For both simulations, the water pressure in the fault zones was assumed to be based on the height of water directly above the fault zone.

The complete loading sequence included the following loading steps:

0) initial in-situ stresses;
I) 3 km of ice loading;
II) 1 km of ice loading;
III) ice retreat forming a thinning of the ice sheet from 0 to 1 km over the area of a potential repository; and,
IV) no surface load.

The vertical in-situ stress used was σ_v=0.0265 Z [MPa], where Z represents the depth below the ground surface in metres. Existing results from the stress measurements were statistically analyzed to provide three possible assumptions for linear variations of minimum horizontal in-situ stresses with depth. The following relations were chosen:

$\sigma_h^{low} = 0.00 + 0.0185\ Z$ [MPa]
$\sigma_h^{medium} = 2.61 + 0.0237\ Z$ [MPa]
$\sigma_h^{high} = 5.50 + 0.02875\ Z$ [MPa]

For each initial stress state, the minimum fault zone strength was chosen to prevent fault zone failure under assumed in-situ stresses. The maximum fault zone strength was chosen such that the entire model was close to elastic response during the maximum load. The variations assumed for the fault zone strength for each of the stress conditions are given in Table 1.

Table 1 Fault zone strengths and corresponding horizontal in-situ stress states used in this study

STRESS σ_h	FAULT ZONE STRENGTH					
	Minimum		Mean		Maximum	
	C [MPa]	ϕ [°]	C [MPa]	ϕ [°]	C [MPa]	ϕ [°]
Low	0.75	17	5.9	17	11	17
Medium	0.75	15	5.3	15	10	15
High	0.75	38	8.9	38	17	38

Results of the sensitivity study were compared in terms of stress distribution, displacement magnitudes, fault zone shear displacements and reactivation ("failure") of fault zones.

The following major findings were obtained from the sensitivity study:

- The high in-situ stress state requires more than twice the fault zone friction angle of the low and medium in-situ stress state to withstand the in-situ stresses. Also, for the mean and the maximum strength cases, the high in-situ stress state results in the highest cohesion of the fault zones as can be seen in Table 1.

- The low in-situ stress state gave a significant reaction to increase in pore pressure. Most of the steeply dipping single fault zones failed throughout the model and maximum shear displacement was one order of magnitude larger than in other simulations - i.e., 0.5 m instead of 0.05 m. The stresses became reoriented and locally, high stress concentrations appear close to failed fault zones.

- The least reaction from the ice load and the pore pressure occurred with the high in-situ stress state.

- For the low in-situ stress state, changes in fault zone strength produced significant effects on the stress distribution. For the medium and the high in-situ stress state, changes in fault zone strength resulted in negligible effects on the stress distribution.

- The increased pore pressure in the fault zones resulting from the introduction of the ice lake reduced the shear deformation in the gently dipping Fault Zone 2, for all combinations of stress and strength except from the low in-situ stress with minimum and mean fault zone strength. The reduced shear deformation caused the stress concentrations in the models to diminish.

TABLE OF CONTENTS

1 INTRODUCTION

As part of the ongoing program for research and development within Swedish Nuclear Fuel and Waste Management Company (SKB), an integrated safety analysis called SKB-91 will be conducted [Swedish Nuclear Fuel and Waste Management Company (1989)]. The analysis will pay specific attention to the glaciation scenario and related phenomena. Therefore, SKB of Sweden in co-operation with Teollisouden Voima OY (TVO) of Finland has initiated studies of the world's ice ages and changing environments and their importance for future glaciations in Fennoscandia [see Eronen and Olander (1990) and Björck and Svensson (1990)]. The integrated safety analysis of SKB-91 will be based on the Finnsjön site of central Sweden. A previous study by Rosengren and Stephansson (1990), illustrated quantitatively possible rock mass response due to glaciation with special emphasis on a future repository located at the Finnsjön site. In the previous study, the rock mass response to glaciation, deglaciation, isostatic movement and water pressure from an ice lake was simulated, using the distinct element computer code UDEC [Itasca (1990)].

The in-situ stresses assumed in the study by Rosengren and Stephansson were derived from a number of hydraulic fracturing tests made at depths of 35 to 500 m. Stresses were extrapolated linearly to a depth of 2000 m. The strength parameters used for the discontinuities were based on reasonable estimates.

The present study was conducted in order to investigate the sensitivity of the model response to in-situ stresses and the fault zone strength. A fault zone represents a weakness plane in the rock mass along which shear movement and separation can occur. The fault zones have an initial peak and a residual shear strength. If the peak shear strength is reached, the fault zones are reactivated in that both the cohesion and the tensile strength of the fault zone are eliminated. The expression "fault zone failure", used in this report, describes the reactivation of the fault zones that occur when the initial peak shear strength of the fault zone is reached. The strength of a failed fault zone is given by its residual strength.

A total of 18 models were studied. Each model was subjected to an ice thicknesses of 3 km, 1 km, and an ice wedge covering half the surface (0-1 km). The in-situ stress/strength-relations for the models are described by a 3 x 3 matrix. This matrix was used for cases with and without an ice lake.

2 REVIEW OF PREVIOUS INVESTIGATIONS

The Finnsjön area, located in central Sweden, is used as a test site for the performance assessment of a waste repository for the Swedish Nuclear Fuel and Waste Management Company, SKB.

Six numerical models have been previously used to simulate the rock mass response to glaciation at Finnsjön [Rosengren and Stephansson (1990)]. The two-dimensional, distinct element computer code UDEC [Itasca (1990)], was used to analyze a model containing nine fault zones. Four of the models had boundary elements acting at the sides and bottom, giving a state of stress in the model which agreed well with an analytical solution. Roller boundaries were applied to the other two models. The induced horizontal stresses from these two models disagreed with the analytical solution. Isostatic movement was also simulated in one of the models.

Each of the six models was subjected to a glaciation load cycle which included the following load steps: I) ice with a thickness of 3 km covers the whole model, II) ice with a thickness of 1 km covers the whole model, III) ice retreating leaving an ice wedge of 0 to 1 km thickness directly above the potential repository, and IV) no remaining surface load. This load cycle was repeated for each model, including an ice lake situated on top of the ice sheet with its accompanying pore pressure distribution in the underlying fault zones.

The results indicated that major stress discontinuities existed in the vicinity of all fault zones, but were most pronounced around the subhorizontal Fault Zone 2. Different boundary conditions gave fault zone failures in different locations and in different orientations. However only small changes were observed when comparing results with and without an ice lake using the same boundary condition. A protection zone (or "stand-off" distance) of about 100 m from the outer boundary of the repository to the discontinuity was suggested. This value was based on results showing that the stress disturbance diminished at this distance from the outer boundary of the discontinuity.

Simulation of pore pressure from an ice lake tended to make the effective stress state in the models more isotropic and diminish the stress concentrations in the vicinity of the fault zones. Future displacements due to glaciation and deglaciation will mainly occur in existing fault zones. The average vertical strain between 250 m and 750 m level below surface was calculated to be 0.3-0.4 mm/m from loading of 3 km of ice.

The model with simulated isostatic movement demonstrated that development of shear failure of the existing fault zones occurs during the melting of the ice. This phenomena has not been found in other models and therefore supports the idea that neotectonics in glaciated areas are of late-glacial origin.

3 METHODOLOGY FOR SENSITIVITY STUDY

For this study, the assumed minimum horizontal in-situ stress and the strength of the fault zones have been varied separately in different models. The reasons and methodology for selecting these parameters are discussed in section 4.5 and 4.6.2 .

The stress state used in the previous study was a result of a linear regression of a total of 40 stress measurement points in one borehole. All measured stress values lying outside the calculated stress function could represent valid stress states. In order to include all possible stress states, these values should be included in a statistical description of the possible stress states in the borehole. Using this assumption for the measured minimum horizontal stress, σ_h, three different stress states were obtained, namely the lowest horizontal stress state, the medium horizontal stress state and finally, the highest horizontal stress state. These stress states will be referred to as the low, medium and high stress state in the following text. A description of the statistical method applied and the stress determination is presented in section 4.5.

For each stress state, three assumptions were made for the strength properties of the fault zones. For each stress state, a set of strength properties of the fault zones was determined so that a non-failing mode was obtained under the in-situ stresses. These sets of strength properties could be described as the "minimum strength" of the fault zones. On the other hand, the strength properties of the fault zones could also be so high that no failure of the fault zones appeared, regardless of the loading condition. However, the strength parameters should not be unreasonably high. This particular set of strength parameters could be described as the "maximum strength". Finally, by taking the arithmetic mean value of the cohesive portion of the strength, a set of "mean strength" properties was obtained. This results in nine (i.e., 3 x 3) stress-strength combinations, as shown in Table 3.1.

Table 3.1 Combinations of in-situ stress states and fault zone strength used in this study

	Minimum Fault Zone Strength	Mean Fault Zone Strength	Maximum Fault Zone Strength
Low Stress	With and with-out ice lake	With and with-out ice lake	With and with-out ice lake
Medium Stress	With and with-out ice lake	With and with-out ice lake	With and with-out ice lake
High Stress	With and with-out ice lake	With and with-out ice lake	With and with-out ice lake

By this, the most extreme situations were described within a range of possible combinations. A comparison to the previous results can also be obtained since the in-situ stress state in the previous study is repeated in this study. The sensitivity of the problem can be investigated for different strengths within each stress case and also by means of the pore pressure effect on the models.

4 DESCRIPTION OF THE MODEL

4.1 MODEL GEOMETRY

The model in this study represents a vertical section which strikes N40°E-S40°W across the Finnsjön site area (Figure 4.1). The section is called "Section A-A" in order to distinguish it from other sections and it is identical to section A-A1 in the previous study, which means that Fault Zone 2 has the same dip throughout the model and an off-set generated by Fault Zone 6, as shown in Figure 4.2.

The area of interest to be covered by the model at the Finnsjön site is about 2.5 km wide and the model depth was chosen to be two km. The shape and dimensions of the entire model and the area of particular interest are described in Figure 4.2. Due to improved computational capacity, the model shape was changed to be rectangular with the same length as in the earlier study. It was assumed that all fault zones were infinitely long and oriented perpendicular to the plane of the analysis. This is a conservative assumption with respect to movement along the strike of the fault zones. Plane strain conditions were assumed, which means that strain perpendicular to the plane of the model section is zero.

4.2 BOUNDARY CONDITIONS

Since the previous study showed that boundary elements at the boundaries of the model gave a better horizontal stress agreement to an analytical solution, all 18 runs in this study were conducted with boundary elements. This means that the force-displacement relation at the boundary is the same as that for a semi-infinite, linear-elastic, isotropic and homogeneous material. The elastic properties of the boundary element domain were the same as for the intact rock blocks used in the distinct element domain.

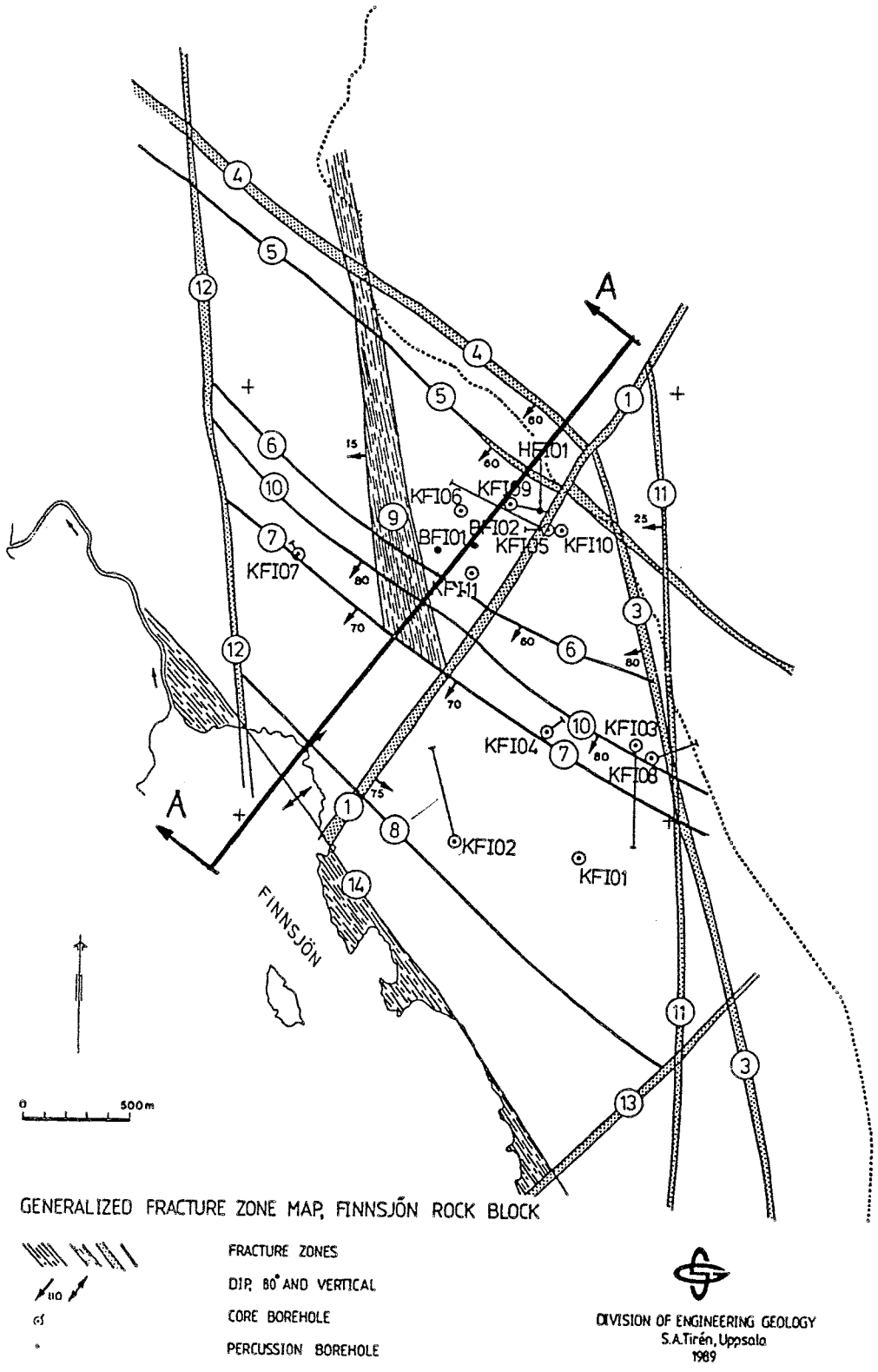

Figure 4.1 Map of the Finnsjön area and the location of section A-A [modified after Ahlbom and Tirén (1989)].

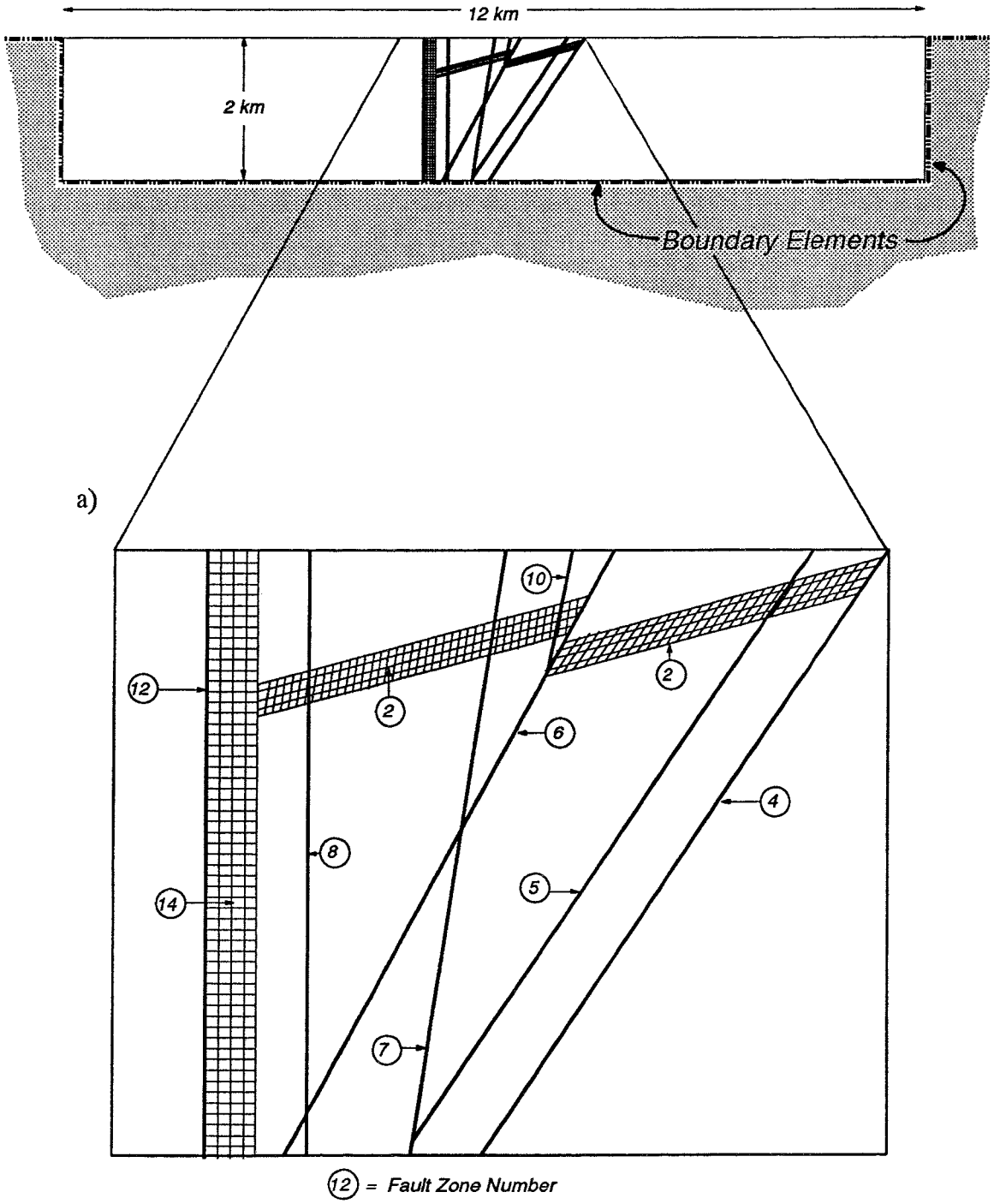

Figure 4.2 Model geometry of the Finnsjön site for a) the whole model and b) detail of the area of interest.

4.3 LOADING CONDITIONS AND SEQUENCES

The modelling sequence was divided into two parallel procedures, i) with ice lake and ii) without ice lake. The different sequences are shown in Figure 4.3. Depending on the presence of the ice lake, the applied vertical stress in each step was as shown in Table 4.1.

Table 4.1 Loading from ice cover and ice lake

Step	Loading Condition	Applied vertical stress (MPa) No ice lake	Ice lake
0	in-situ stress state	-	-
I	uniform load of 3 km ice	27	30
II	- " - of 1 km ice	9	10
III	ice wedge	0-9	0-10
IV	no load	-	-

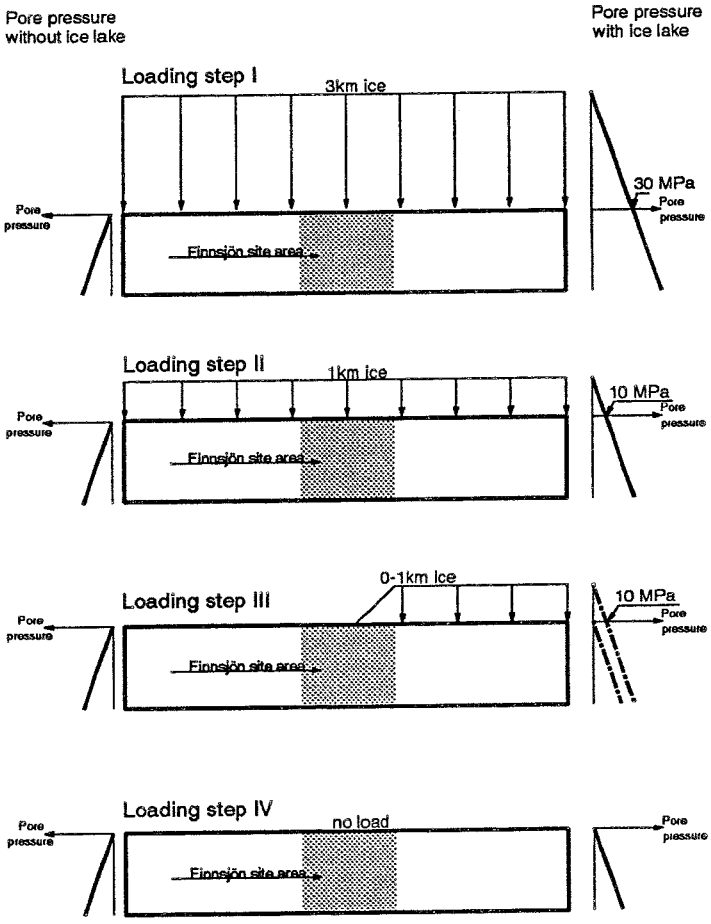

Figure 4.3 Loading steps and pore pressure distribution without ice lake (left) and with ice lake (right).

4.4 PORE PRESSURE CONDITIONS

The effect of pore pressure and static water load has been included in all models of this study. The pore pressure distribution for the models without the ice lake was assumed to be hydrostatic, with zero pressure at the ground surface and 20 MPa at base of the model as shown in Figure 4.3. The pore pressure was set to be 30 MPa at the ground surface for 3 km of ice and 10 MPa for 1 km of ice in the runs with the ice lake. The lake was assumed to be located on top of the ice sheet. For the loading step where only part of the model is covered with ice, the pore pressure ranges from 0 to 10 MPa at the ground surface, depending on the ice thickness.

Notice that pore pressures in the model only exist in fault zones and that the intact blocks are assumed to be impermeable in the UDEC code. Density for water was assumed to be 1000 kg/m^3. No water flow was simulated.

4.5 IN-SITU STRESSES

Stress measurements were conducted at 40 different points down to 500 m depth in borehole KFI06 at the eastern part of the extension of Fault Zone 2 [Bjarnason and Stephansson (1988)]. The measurements were conducted with hydrofracturing and the stress determination was based on 26 of the tests. Regression analysis of stress magnitudes versus depth gave:

$$
\begin{aligned}
\sigma v &= 0.0265\ Z && \text{[MPa]} && \text{(estimated)} \\
\sigma h &= 2.6 + 0.0237\ Z && \text{[MPa]} && r=92\% \\
\sigma HI &= 6.2 + 0.0416\ Z && \text{[MPa]} && r=85\% \\
\sigma HII &= 2.4 + 0.0412\ Z && \text{[MPa]} && r=89\%
\end{aligned}
\qquad (4.1)
$$

where σv = vertical stress (weight of overburden),
σh = minimum horizontal stress,
σHI = maximum horizontal stress by first breakdown method,
σHII = maximum horizontal stress by second breakdown method,
Z = depth in metres, and
r = correlation coefficient.

A linear regression of the maximum and minimum horizontal stress above and below Fault Zone 2 were conducted by Bjarnason and Stephansson (op. cit.). Due to the low number of measuring points for each regression line and the relatively large scatter of maximum horizontal stress magnitudes below Fault Zone 2, the results were not conclusive. In order to present the stress data versus depth, the authors lumped all the 26 data points to obtain the following results.

- The maximum horizontal stress, σH, is larger in magnitude than the vertical stress at all depths.
- The minimum horizontal stress, σh, becomes smaller than the vertical stress at a depth of about 500 m.
- A stress field with thrust fault conditions (σv < σh < σH) from the ground surface down to 500 m is changing to strike-slip condition (σh < σv < σH) below 500 m depth.

In the regression analysis of the test data from Finnsjön, the variation in orientation of σH and σh was not considered.

A compilation of all stress measurements in the Baltic Shield and the Caledonides is found in the Fennoscandian Rock Stress Data Base (FRSDB) [Stephansson et al., (1986)]. When all existing data points from various measurement techniques are compiled and subjected to a regression analysis, the results are:

$$\sigma H = 5 + 0.032\ Z \quad [MPa]$$
$$\sigma h = 2 + 0.028\ Z \quad [MPa] \qquad (4.2)$$

A regression analysis of only hydraulic fracturing data in FRSDB gives;

$$\sigma H = 2.8 + 0.0399\ Z\ [MPa] \quad r=79\%$$
$$\sigma h = 2.2 + 0.0240\ Z\ [MPa] \quad r=81\% \qquad (4.3)$$

The vertical stress σv corresponds to the weight of the overburden - i.e., σv = 0.027 Z.

A comparison of regression analysis of test results from Finnsjön and FRSDB demonstrates several interesting features. For maximum horizontal stress, results of stress determinations with the first breakdown method are in fair agreement with all data in FRSDB, eq. (4.2). The same observation holds for comparison between σH by the second breakdown method and hydraulic fracturing results in FRSDB. In conclusion, the stress profile determined at Finnsjön is in fair agreement with the average stress condition in the Baltic Shield.

The facts that stress data from Finnsjön are scattered and limited to the depth of 500 m and modelling requires stress estimation to a depth of two km, call for statistical processing of test data. A regression analysis based on the least square method has been applied to the Finnsjön data and performed by Magnus Liedholm, VBB/VIAK (personal communication). A linear function of minimum horizontal stresses versus depth and a function of minimum horizontal stress versus power of depth were tested. It turned out that the power law fit the data slightly better than the linear function. The statistical analyses were performed only for the minimum horizontal stress versus depth since that is the most interesting variable to the stress condition of the two-dimensional model at section A-A in Figure 4.1.

Since a) the power law was only slightly better than linear relation, and b) it is more convenient to specify a linear relation, a linear statistical model was used in the model to

specify the minimum horizontal stress for a depth down to 2000 m. This assumption resulted in:

$$\sigma h = 2.6078 + 0.0237269\ Z\ [MPa] \quad r^2=85\% \tag{4.4}$$

where r^2 is the coefficient of determination, obtained by dividing the explained variation with the total variation. This relation was used as the medium horizontal in-situ stress state in this study.

Three different confidence intervals (90, 95 and 99%), were tested for the given population of σh values and the 99% confidence interval was applied. The curved upper and lower bound of the confidence from the regression analysis of the minor horizontal principal stress have been approximated to straight lines. Hence, the upper and lower bound and the mean value of the minimum horizontal stress are given in eq. (4.5) and are depicted in Figure 4.4. These functions are used as in-situ stresses in the modelling of the Finnsjön site in this study.

$$\begin{aligned} \sigma_h^{low} &= 0.00 + 0.0185\ Z\ [MPa] \quad \text{(linear approximation)} \\ \sigma_h^{medium} &= 2.61 + 0.0237\ Z\ [MPa] \quad \text{(linear regression model)} \\ \sigma_h^{high} &= 5.50 + 0.0288\ Z\ [MPa] \quad \text{(linear approximation)} \end{aligned} \tag{4.5}$$

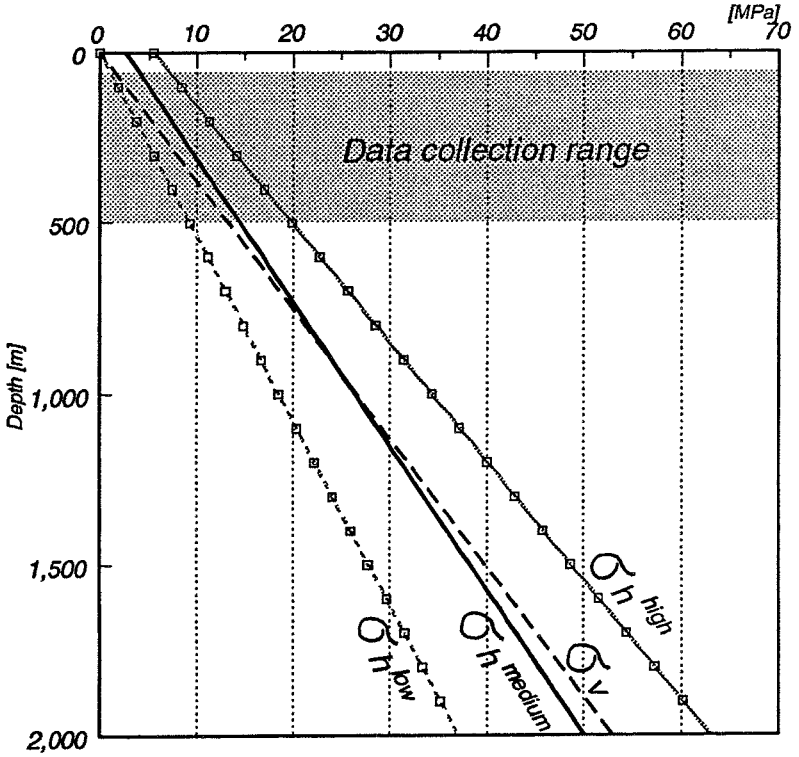

Figure 4.4 Predicted bounds and estimate of minimum principal stress, σh, and predicted vertical stress, σv, versus depth at Finnsjön assumed for this study.

In order to visualize the uncertainties in the statistical analysis and the prediction of stresses at great depth the range of data collection has been marked in Figure 4.4. An extrapolation to four times the depth of sampling means uncertainties. At the time when the stress measurements were conducted in late 1987, the multi-hose instrumentation for hydrofracturing allowed fracturing down to 500 m. The new equipment, now existing at Luleå University of Technology, can reach 1000 m and the new data acquisition system allows more sophisticated data recording and processing. Hence, to validate the assumption of stress versus depth, an extension of the stress measurement profile from 502 m level to 1000 m level is recommended.

4.6 MATERIAL PROPERTIES

4.6.1 Properties of Intact Rock Material

The rock blocks (i.e., the rock material between the fault zones) were assumed to behave as linear-elastic, isotropic and homogeneous material. This means that the intact rock material has unlimited strength. The deformation of the material is linearly proportional to the stress acting on the material. The properties of the rock blocks used for the models were

Density, ρ [kg/m^3]	2650
Young's modulus, E [GPa]	40
Poisson's ratio, υ	0.2

4.6.2 Properties of Fault Zones

The following assumptions were made for the fault zones.

- All fault zones strike perpendicular to the plane of the model.
- The location and orientation of the fault zones are in accordance with the AutoCAD drawings provided by SGAB, Uppsala.
- The strength of the fault zones are defined by the Coulomb slip criterion. When shear or tensile strength of the fault zone is reached it reactivates in that it looses its cohesion and tensile strength. The initial tensile fault zone strength is assumed to be zero. All fault zone properties are hypothetic, i.e. laboratory or field testing have not been conducted.
- All fault zones are assumed to have identical strength parameters, which was not the case in the previous study by Rosengren and Stephansson (1990).

- During any single simulation model, all fault zones have the same shear stiffness of 3.33 GPa/m and normal stiffness of 10 GPa/m except for Fault Zones 2 and 14 which have a shear stiffness of 0.33 GPa/m and a normal stiffness of 1 GPa/m.

For this study, it was decided to use both friction and cohesion for the fault zones. The reasons for this were as follows.

- No peak strength could be achieved by only using friction since the constitutive model used for the fault zones (JCONS 5) reduces the cohesion and the tension to zero as the fault zone fails. Friction would have to be too high if the cohesion was set to zero. When using a cohesion of the same range as in the previous study (0.5 and 1.0 MPa), the required friction angles were within reasonable ranges.

- By only using cohesion, the total strength of the fault zone would be lost since the cohesion drops to zero when the strength is reached (for the constitutive relation used in this study).

For each in-situ stress state (low, medium and high) the fault zone strength was calculated so that the minimum fault zone strength did not result in failure of fault zones under the applied in-situ stress state. The minimum strength requirements were calculated for each fault zone based on their dip and location. The fault zone cohesion was kept constant (0.75 MPa) in all stress cases while the friction angles, required to prevent failure of fault zones, were calculated.

However, the maximum fault zone strength should prevent the model from failure under the biggest load ever applied to the model. The most pronounced effects on the model occur during load step I (i.e., applying 3 km of ice to the ground surface). It was assumed that the maximum fault zone strength should give a near elastic response for this load case. The failure mechanism in the model involved shear failure from bending movements, with some minor local failures as a result. Therefore, the decision was made that the maximum fault zone strength should reduce the amount of failures from the minimum fault zone strength cases by 90% . In order to make the changes of fault zone strength in a clear way, the friction angle determined for the minimum fault zone strength was kept constant and only the cohesion was changed.

The UDEC code was modified to present the percentage of failed fault zones in the model. Thereby, a value for the degree or extent of failure could be presented.

After both the minimum and maximum strength were determined the mean strength was calculated as the mean value of the two extremes. The complete set of strength parameter values is shown in Table 4.2.

Table 4.2 Strengths of fault zones used for the different in-situ stress states.

STRESS STATE	STRENGTH OF FAULT ZONES					
	Minimum		Mean		Maximum	
	ϕ [°]	C [MPa]	ϕ [°]	C [MPa]	ϕ [°]	C [MPa]
Low	17	0.75	17	5.9	17	11
Medium	15	0.75	15	5.3	15	10
High	38	0.75	38	8.9	38	17

Simplified, the procedure to obtain the different strength values can be described as follows:

1) "Minimum strength" case: Choose cohesion, C=0.75 MPa and determine the minimum friction angle required to prevent any failure in the fault zones for the in-situ stresses.

2) "Maximum strength" case: Keep the friction angle determined from 1) above and determine a cohesion which gives a 90% reduction of the failures induced for the "Minimum strength" case for maximum load (i.e., 3 km ice).

3) "Mean strength" case: Keep the friction angle from 1) above and calculate the arithmetic mean value for the cohesion from 1) and 2) above.

This procedure was repeated for all in-situ stress cases.

5 RESULTS

5.1 PRESENTATION OF RESULTS

Results are presented as plots provided directly from the UDEC runs and as post-processed data - i.e., diagrams of stress distributions for selected sections of the model. The results are presented for the low, medium and high in-situ stress state and associated fault zone strengths. Each model is numbered as listed in Table 5.1.

Table 5.1 Model number and assumed conditions for the Finnsjön Sensitivity Study

Model No	Ice Lake Yes/No	In-situ Stress State[1]	Strength of Fault Zones[2]
1	No	Low	Minimum
2	No	Low	Mean
3	No	Low	Maximum
4	No	Medium	Minimum
5	No	Medium	Mean
6	No	Medium	Maximum
7	No	High	Minimum
8	No	High	Mean
9	No	High	Maximum
10	Yes	Low	Minimum
11	Yes	Low	Mean
12	Yes	Low	Maximum
13	Yes	Medium	Minimum
14	Yes	Medium	Mean
15	Yes	Medium	Maximum
16	Yes	High	Minimum
17	Yes	High	Mean
18	Yes	High	Maximum

[1] see eq. (4.5)

[2] see Table 4.2

Major and minor principal stresses versus depth and shear (σ_{xy}) stresses versus depth are presented for two vertical sections (x=175 m, x=-540 m) shown in Figure 5.1.

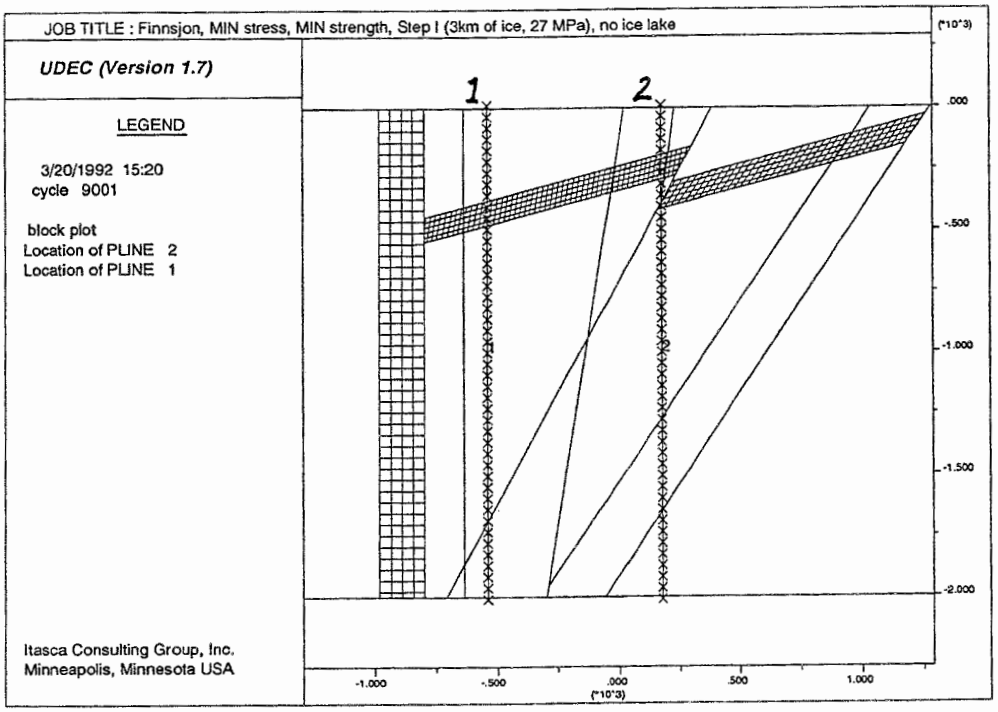

Figure 5.1 Location of the two stress profiles named PLINE 1 (x=-540 m) and PLINE 2 (x=175 m).

Typical results are presented for all in-situ stress states, together with a more detailed presentation of the results from the low in-situ stress state.

In UDEC, compressive stresses are negative. Therefore, maximum principal stress, given in the legends of the UDEC plots, represents the lowest compressive or the highest tensile principal stress. Consequently, the minimum principal stress represents the highest compressive stress.

The stresses presented in the plots are total stresses in the solid blocks. The normal and the shear stress in the fault zones in the models and in the analytical calculations presented later, are effective stresses - i.e., reductions are made due to existing pore pressures.

5.2 LOW IN-SITU STRESS STATE

The minimum stress state was used to model No's. 1, 2, 3, 10, 11 and 12. Of these, model No's. 10, 11 and 12 included the pore pressure effects from the ice lake (see Table 5.1).

5.2.1 Stress

A series of plots of principal stress distribution in the model are shown in Figures 5.2 and 5.3. The plots represent all four loading steps for the case of minimum fault zone strength without the presence of an ice lake. Figure 5.2 shows that Fault Zones 2 and 14 have a major impact on the distribution of principal stresses during loading steps I and II (3 km ice and 1 km ice). Loading step III (ice wedge) gives a more gradual rotation of the principal stresses caused by the non-uniform strip load (Figure 5.3a). For loading step IV (no load), the magnitude and distribution of the principal stresses is similar to the in-situ stress state (not shown).

When looking at the stress situation during the first loading step (3 km ice), the following is noticed. For the case without an ice lake, the horizontal stress component is disturbed in the vicinity of Fault Zone 2. The vertical stress component was disturbed in the vicinity of Fault Zone 14. The two stress profiles at x=-540 m and x=175 m indicate stress anomalies for the principal stresses at their intersection of Fault Zone 2. However, no significant differences were found in the results for models simulating different strength parameters (Figure 5.4). The presence of shear stress (σ_{xy}) in the models depicted in Figure 5.4 indicates rotation of the principal stresses from the original horizontal/vertical orientation.

For the case of the ice lake, the stress anomalies in the vicinity of Fault Zone 2 are of a much lower magnitude compared to the case of no ice lake. Pronounced stress anomalies now appear in the bottom of the model for the minimum and mean strength case. These two cases exhibit varying degree of stress rotation throughout the whole model depth along the two profiles. This finding is confirmed by the presence of shear stress (σ_{xy}) shown in Figure 5.5a,b. The model with maximum fault zone strength show only minor influence on principal stresses along the two profiles (Figure 5.5c).

The stress field in the model is sensitive to the introduction of an ice lake. With the ice lake present, the model is also sensitive to variation in fault zone strength properties.

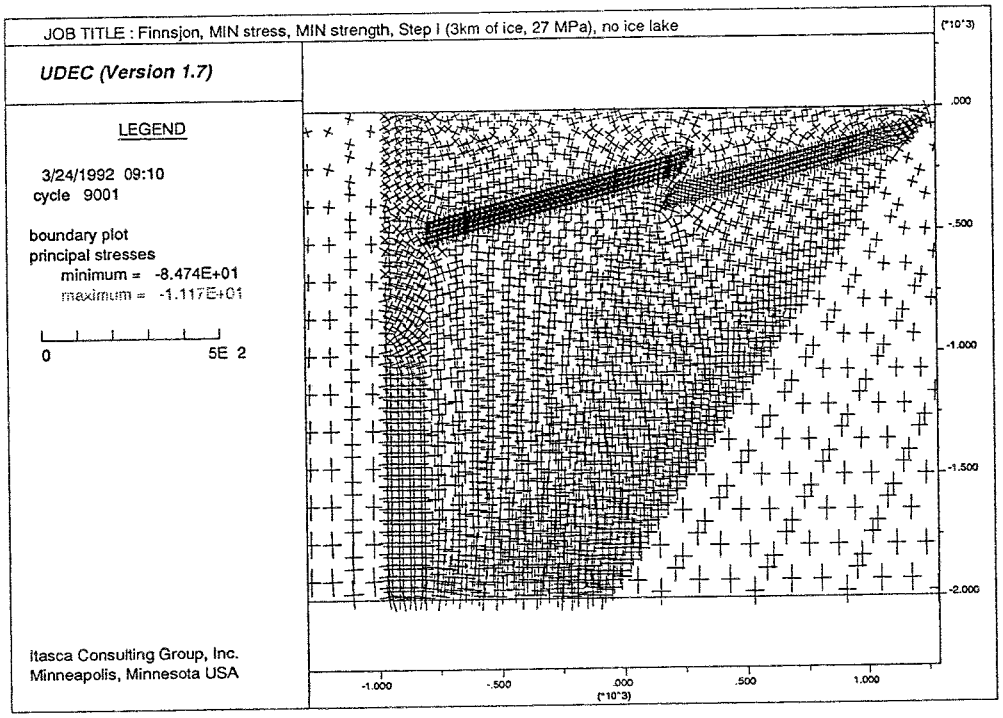

a)

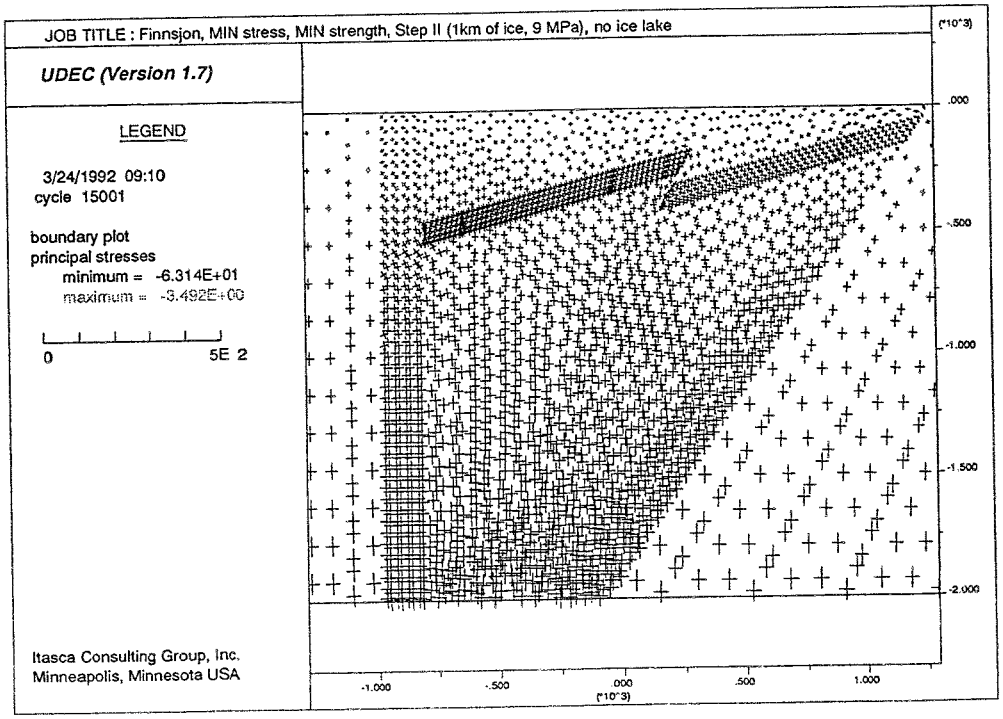

b)

Figure 5.2 Principal stress distribution. Low stress state, minimum strength without ice lake. a) Loading step I (3 km ice), b) Loading step II (1 km ice).

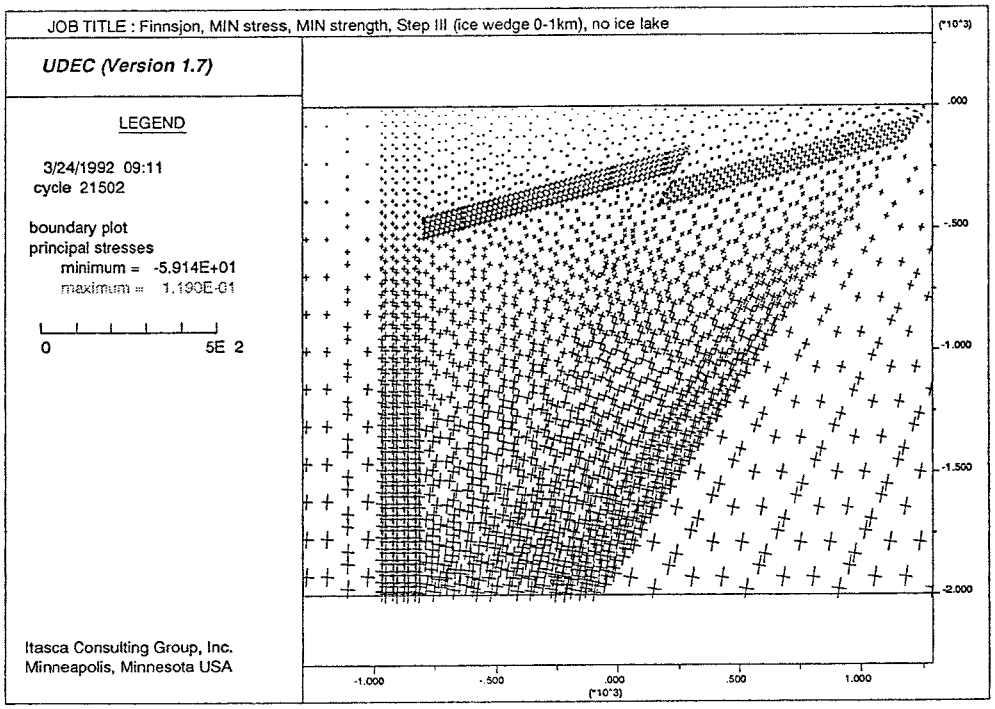

a)

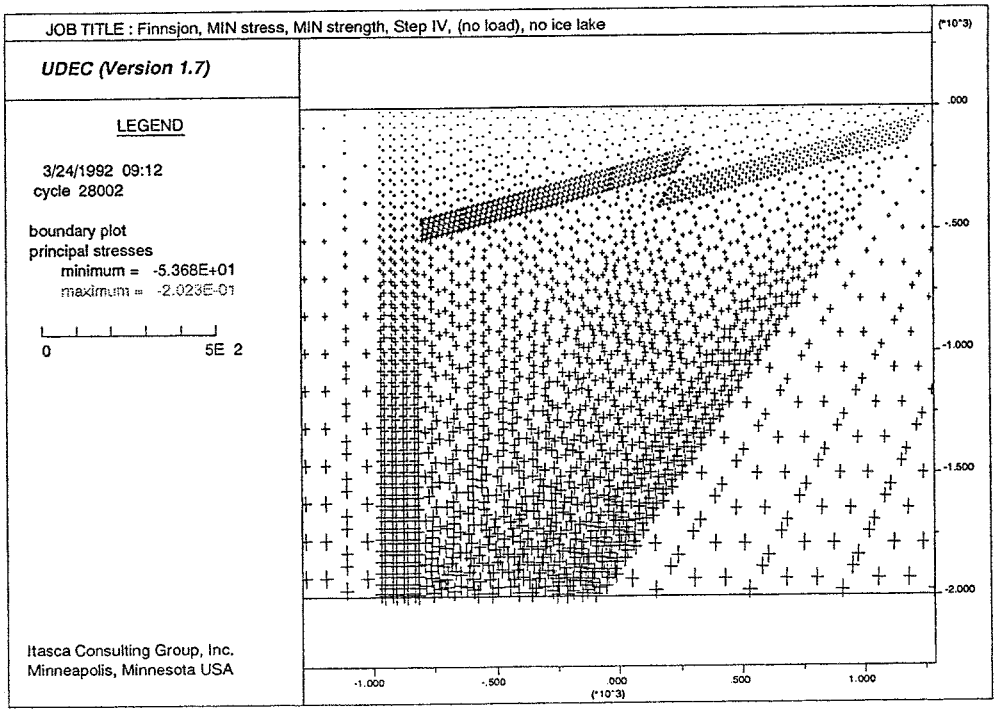

b)

Figure 5.3 Principal stress distribution. Low stress state, minimum strength without ice lake. a) Loading step III (ice wedge), b) Loading step IV (no load).

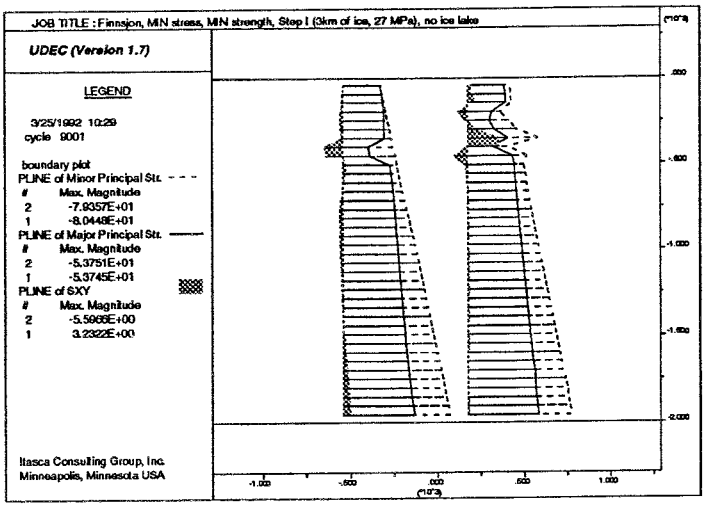

a)

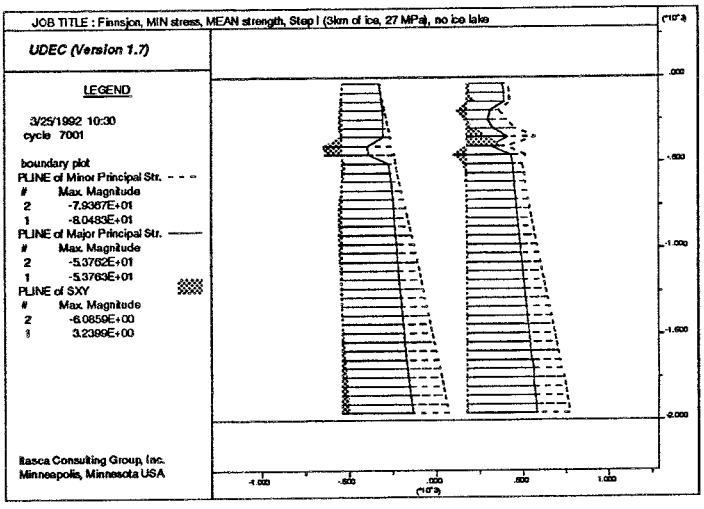

b)

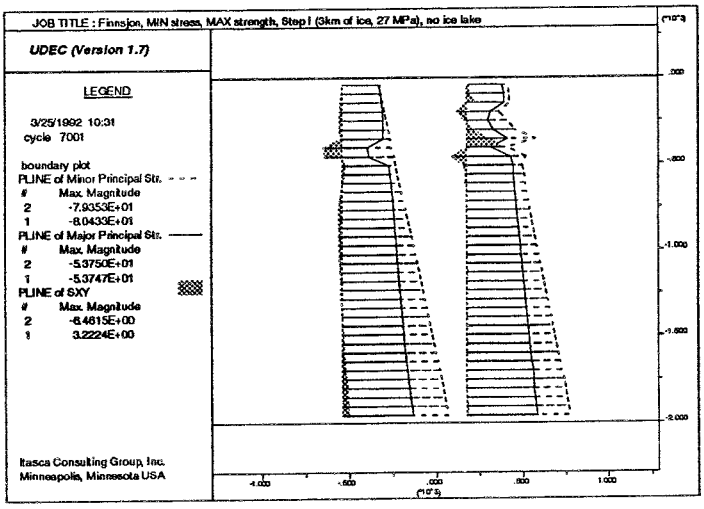

c)

Figure 5.4 Principal stresses and shear stress (σxy) versus depth for low stress state without ice lake, loading step I. a) minimum (Model 1), b) mean (Model 2) and c) maximum (Model 3) strength of fault zones.

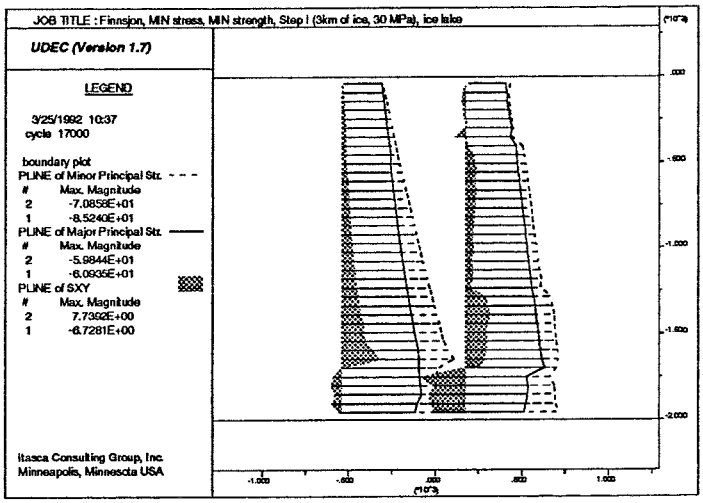

a)

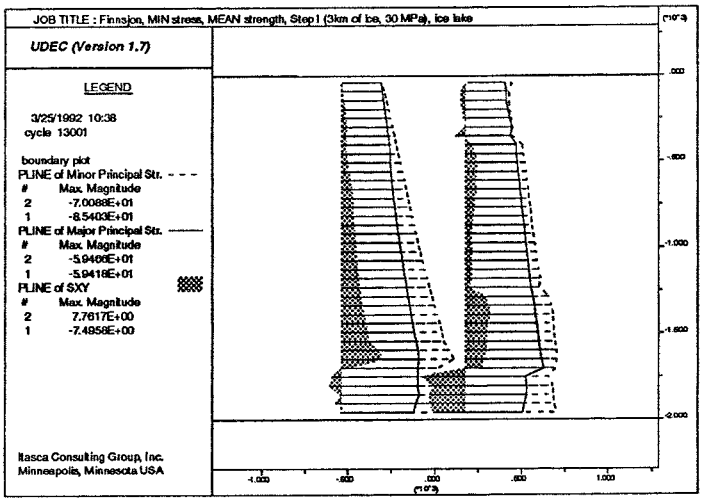

b)

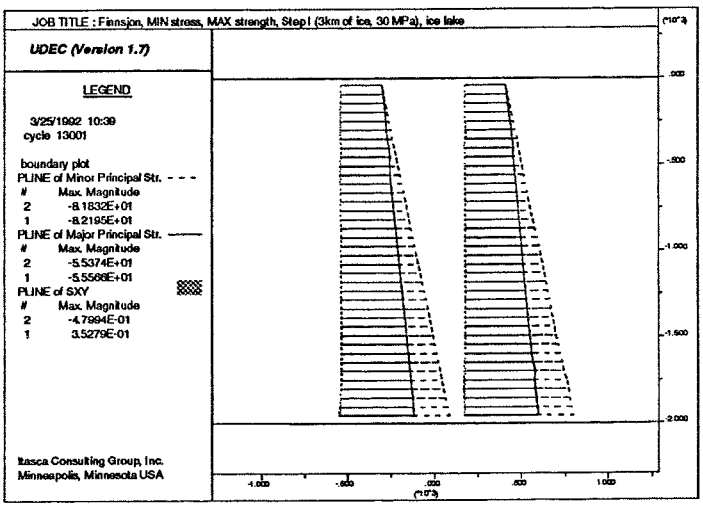

c)

Figure 5.5 Principal stresses and shear stress (σxy) versus depth for low stress state with ice lake, loading step I. a) minimum (Model 10), b) mean (Model 11) and, c) maximum (Model 12) strenght of fault zones.

5.2.2 Displacements

Figures 5.6 and 5.7 show the displacement field for the case of minimum fault zone strength without the ice lake for loading steps I-IV (Model 1). The general displacement trend is directed downward. The effect from the finite strip load makes the displacement field inclined slightly toward the center of the model. The maximum displacement of 2.5 m occurs during loading step I (Figure 5.6). However, the third loading step (ice wedge) results in a different displacement field with a small uplift behind the retreating ice front (Figure 5.7b).

The strain along a 500 m long vertical section in the center of the model between depth of 250 and 750 m was calculated to be approximately 0.9 mm/m during loading step I.

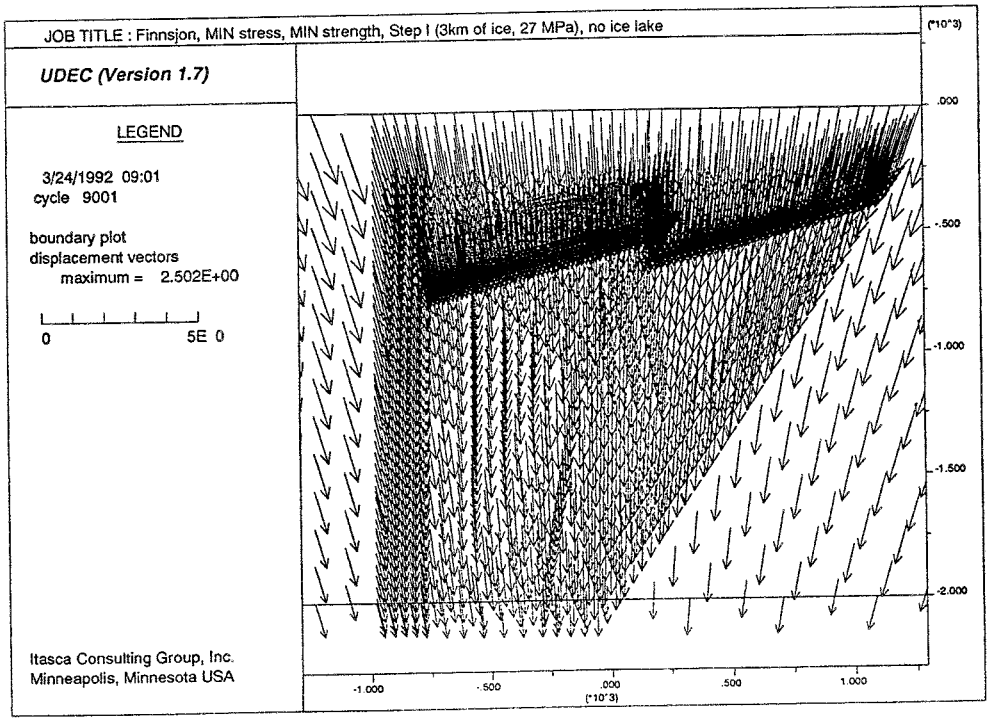

Figure 5.6 Displacements in Model 1 from loading step I (3 km ice). Low stress state, no ice lake and minimum strength of fault zones.

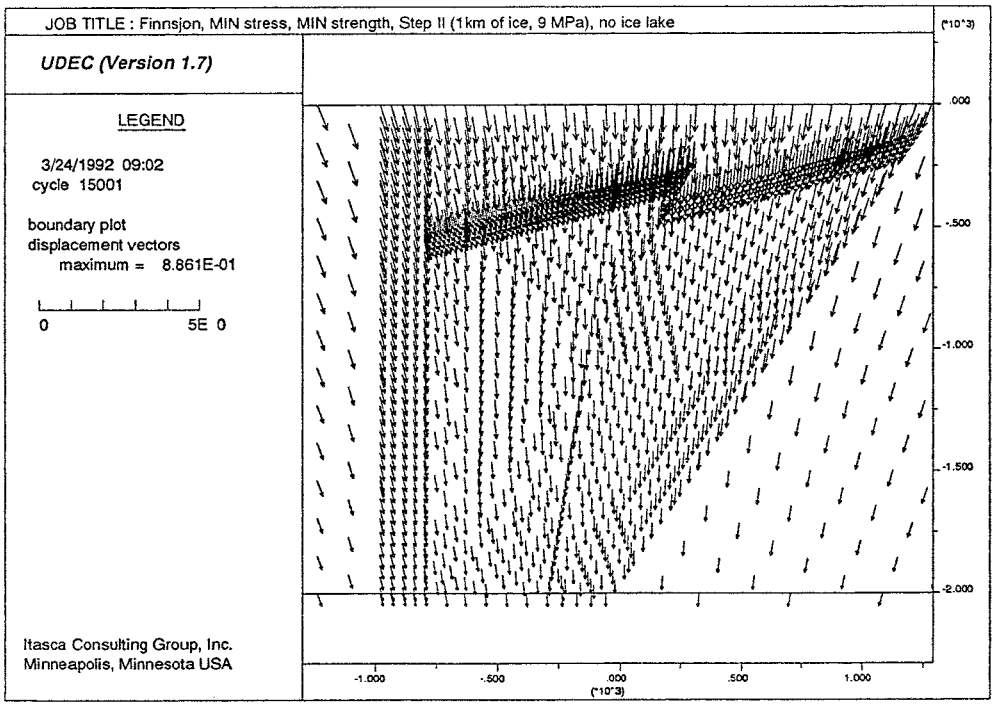

a)

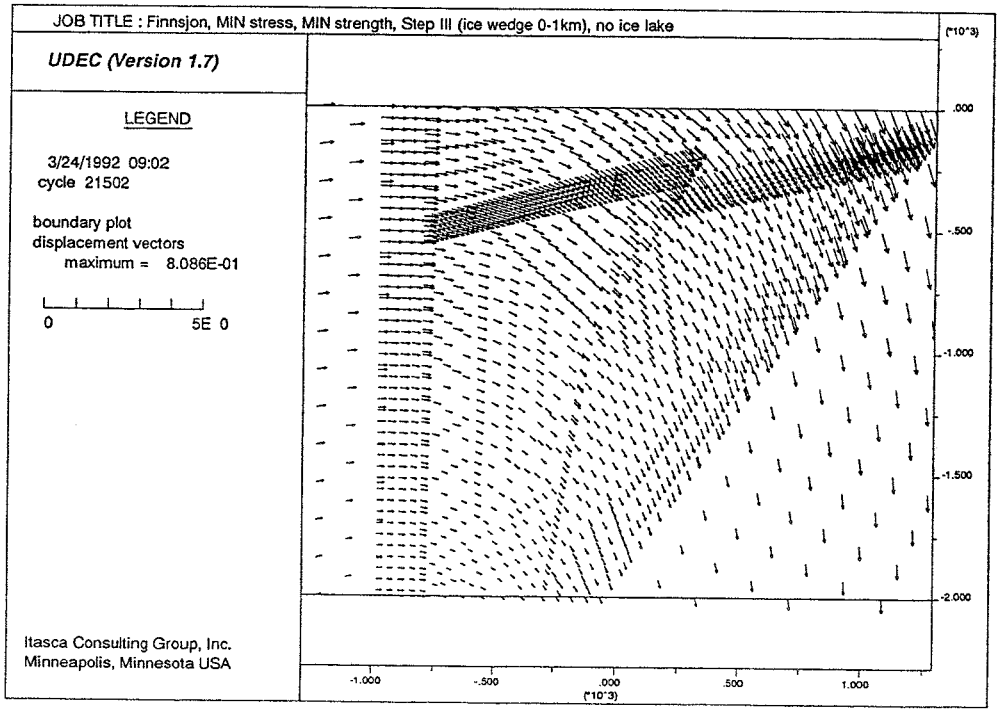

b)

Figure 5.7 Displacements in Model 1 from a) loading step II (1 km ice) and b) loading step III (ice wedge). Low stress state, no ice lake and minimum strength of fault zones.

5.2.3 Shear Displacements on Fault Zones

For the cases of no ice lake (Models 1, 2 and 3), the models behave in general as all models do without the ice lake during the first loading step. Figure 5.8 shows the shear displacement on fault zones for the cases with different strength of fault zones and no ice lake. The dominating shear deformation of Fault Zone 2 can be characterized as a homogenous, primarily elastic shearing with maximum magnitudes of roughly 4.6 cm for all three strength cases. Also, the more steeply dipping fault zones (6, 12 and 14) are subjected to shearing movements. The shear displacements on fault zones are mainly within the elastic range - i.e., they are insensitive to changes of the fault zone strength. For the subsequent loading steps (II-IV), the maximum shear displacements decrease and relocalize. A shear concentration at Fault Zone 12 for loading step III (ice wedge) can be found. When the model is unloaded (step IV), no shear displacements remain except for Fault Zone 12, on which some residual displacements can be found for the cases of minimum and mean fault zone strength.

When the ice lake is introduced, the shear displacements increase drastically for the minimum and mean strength cases (Figure 5.9). Major shearing is located at Fault Zones 4, 5, 6 and 8 during loading step I, with maximum shear displacement of approximately 0.5 m. For the following loading steps, maximum shear displacements remain at about 0.5 m. Additional shearing occurs in Fault Zone 12 for loading step II (1 km ice), minimum and mean strength cases and in Fault Zone 2 for loading step III (ice wedge), minimum strength case. Since most shear displacements are inelastic, they remain after unloading (loading step IV). However, almost zero shear displacements are recorded in the different loading steps for the case of maximum strength.

Based on these results, it can be concluded that the shear displacement in fault zones is sensitive to the introduction of the ice lake. The model has low sensitivity to changes in strength properties for the case without the ice lake. However, when an ice lake is introduced, the models show large differences in shear displacements for fault zones as a function of strength properties.

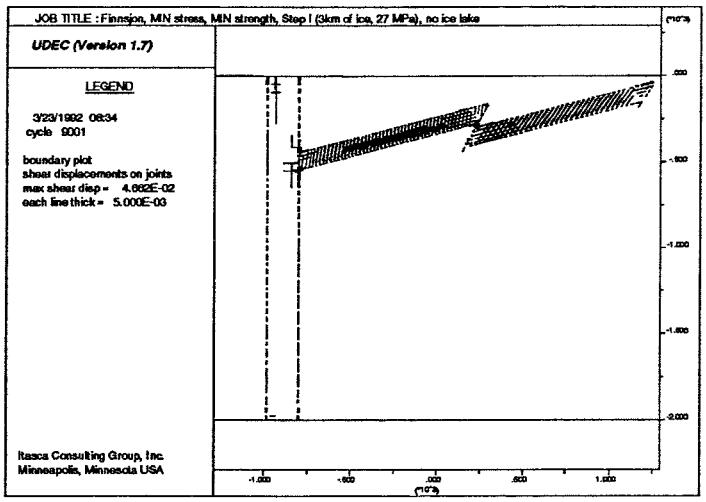

a)

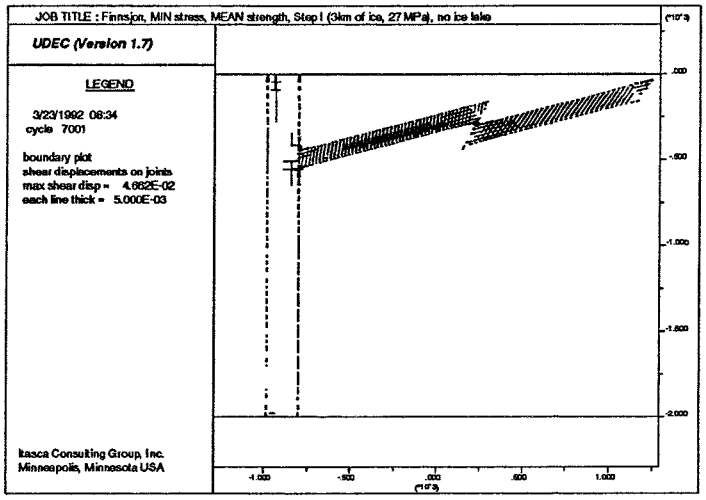

b)

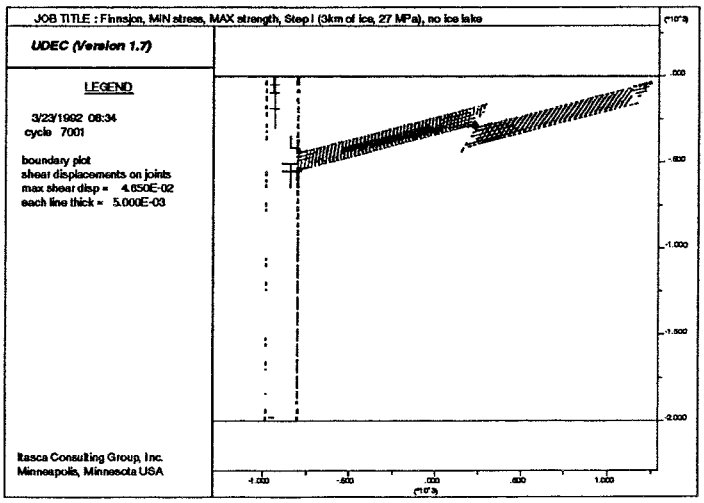

c)

Figure 5.8 Shear displacement on fault zones for low in-situ stress and no ice lake, loading step I (3 km ice). a) minimum (Model 1), b) mean (Model 2) and c) maximum (Model 3) fault zone strength.

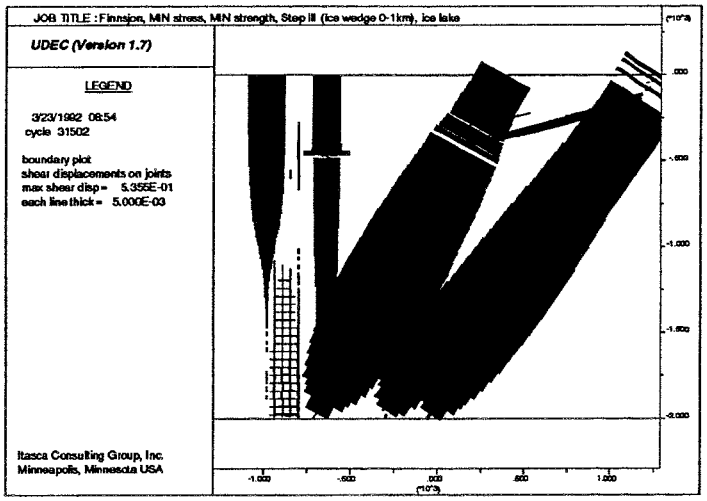

a)

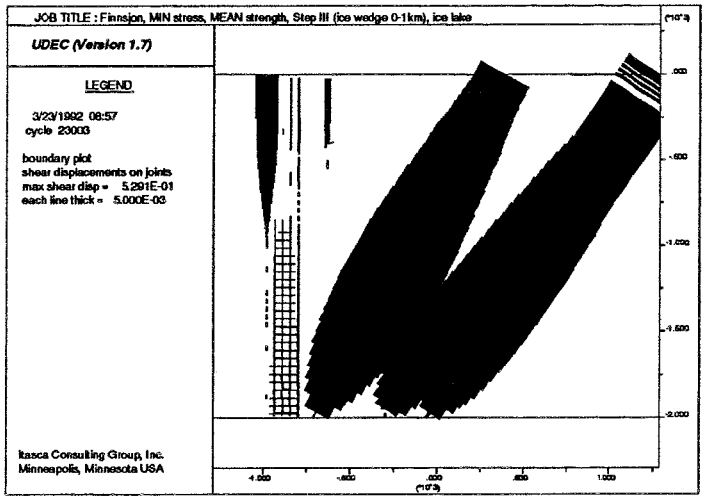

b)

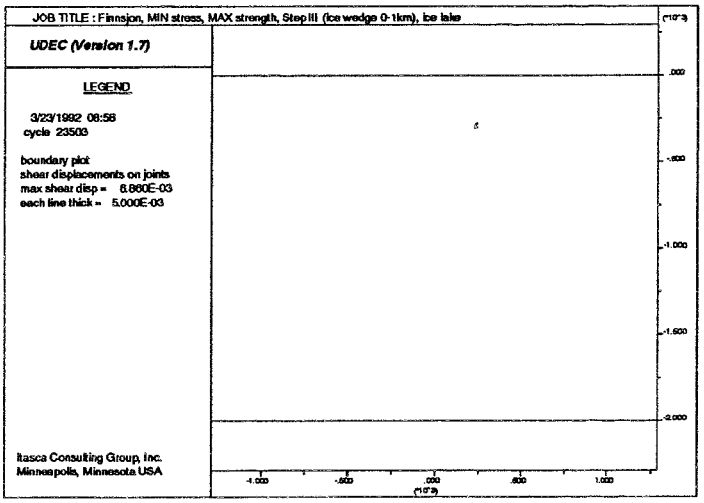

c)

Figure 5.9 Shear displacement on fault zones for low in-situ stress and ice lake, loading step III (ice wedge). a) minimum (Model 10), b) mean (Model 11) and c) maximum (Model 12) strength of fault zones.

5.2.4 Failure of Fault Zones

For the case of no ice lake, failure of fault zones occurs during the first loading step (3 km ice) and no additional failure during the subsequent loading steps (II-IV) is evident. The failures are located along Fault Zones 4 and 6 at their intersection with Fault Zones 2 and 12. For the case of minimum strength, Fault Zone 12 fails throughout the model. Increasing the fault zone strength gives less extension of failures. This indicates that failures in the model, without ice lake, are sensitive to strength properties, as shown in Figure 5.10.

Faults in models simulating an ice lake fail mainly during the first loading step (3 km ice), except for the minimum strength case which shows additional failure of Fault Zone 2 during loading step III (ice wedge). Increasing the fault zone strength from minimum to mean strength gives only a slight reduction of fault zone failures. However, increasing the strength from mean to maximum results in an almost unfailed model, as shown in Figure 5.11.

The introduction of an ice lake results in a major increase of failed fault zones. Table 5.2 shows the percent failure of total fault zone length for each strength and pore pressure (i.e., ice lake/no ice lake) case for loading step IV (no load).

Table 5.2 Percentage of failed fault zone length to total fault zone length for the low stress state, (loading step IV, no load)

Strength of fault zones	Model No.	No ice lake	Model No.	Ice lake
Minimum	1	3.7%	10	27.1%
Mean	2	2.0%	11	19.8%
Maximum	3	0.2%	12	0.5%

As can be seen from Table 5.2, the model is sensitive to the introduction of an ice lake. If the ice lake is present, the model also is sensitive to changes of the fault zone strength.

The failure of fault zones during the first loading step (3 km ice) is concentrated at fault zones with higher stiffness than their neighboring fault zones. Both Fault Zones 2 and 14 are simulated as systems of regularly spaced joints with one order of magnitude lower stiffness in both normal and shear directions as compared to the fault zones in general, as described in section 4.6.2. Fault zones tend to fail at intersections with fault zones with lower stiffness, such as Fault Zones 2 and 14. The vertical Fault Zone 12 that fail all the way down to the bottom of the model behaves as a stiffer boundary to the soft Fault Zone 14.

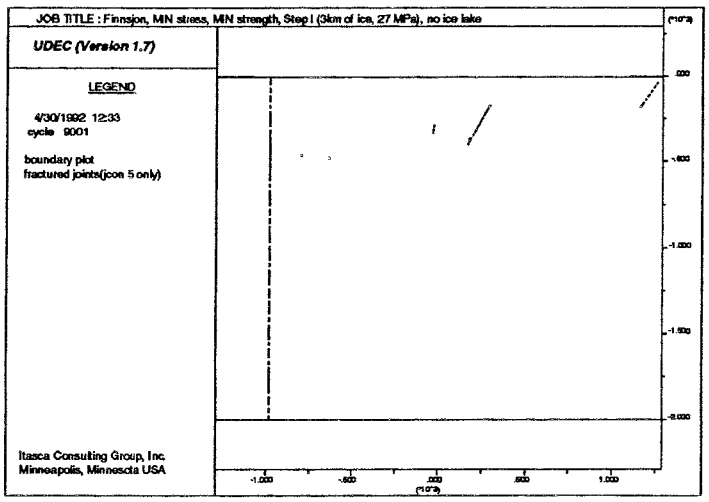

a)

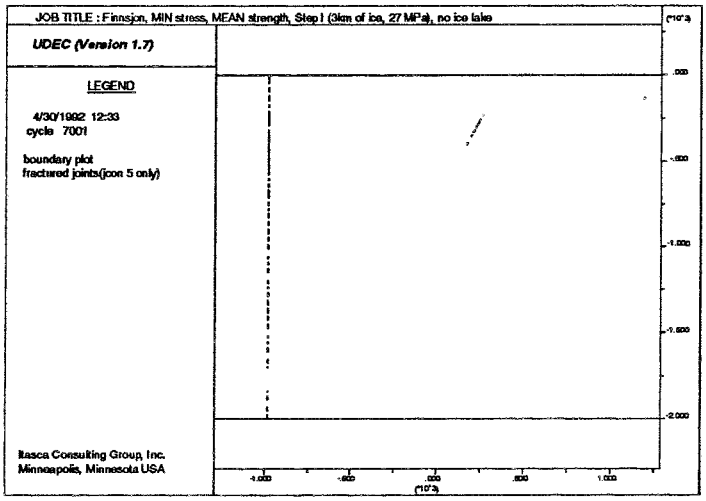

b)

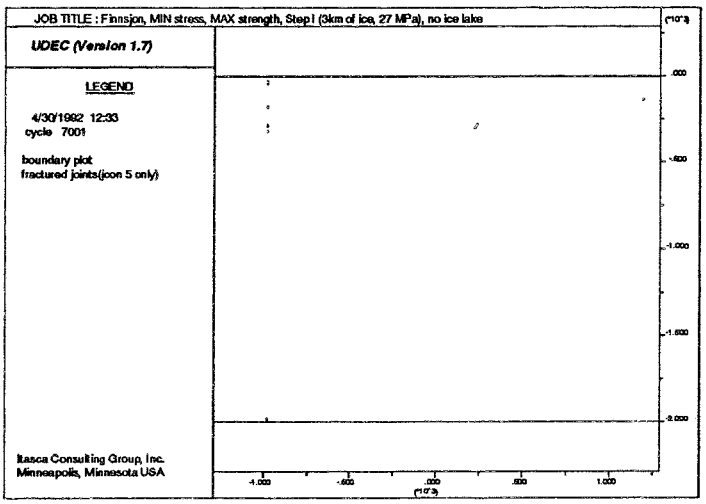

c)

Figure 5.10 Failure of fault zones for loading step I (3 km ice) with low in-situ stress and no ice lake. a) minimum (Model 1), b) mean (Model 2) and c) maximum (Model 3) strength of fault zones.

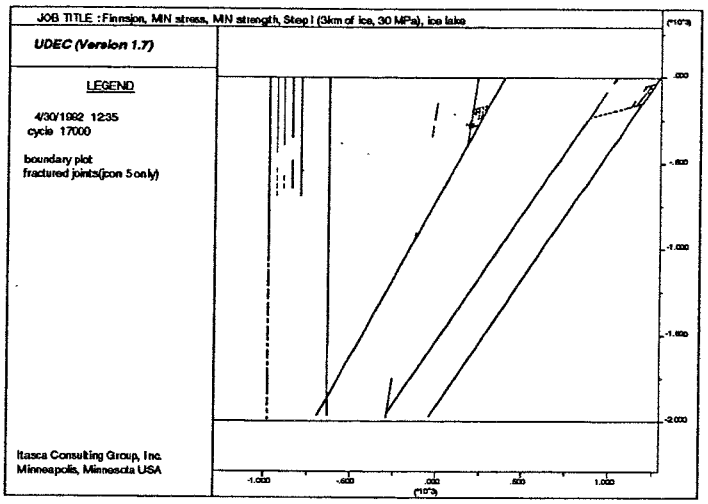

a)

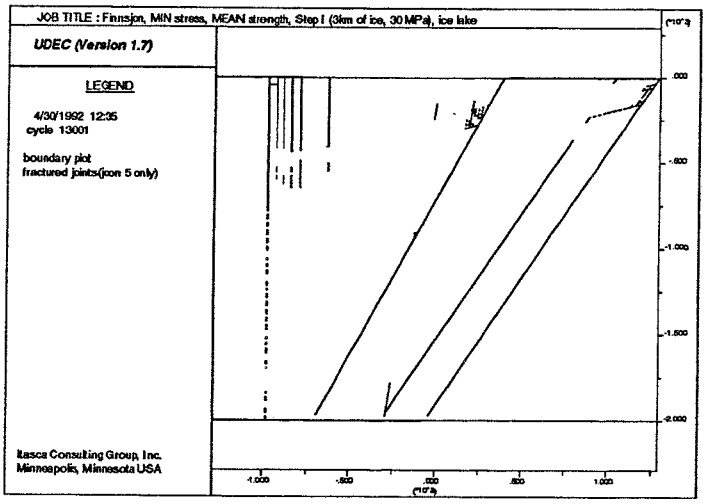

b)

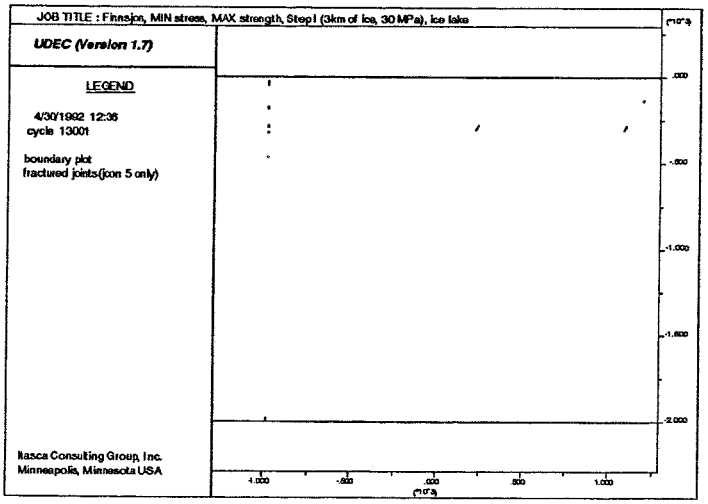

c)

Figure 5.11 Failure of fault zones with low in-situ stress and ice lake for loading step I (3 km ice). a) minimum (Model 10), b) mean (Model 11) and, c) maximum (Model 12) strength of fault zones.

5.2.5 Discussion and Conclusions

Based on the results presented for the low in-situ stress state, the following general conclusions can be drawn.

1) The models are sensitive to increases in pore pressure. Large differences in the model response can be seen when comparing models with and without an ice lake situated on top of the ice sheet.

2) The models are relatively insensitive (3.7% to 0.2%, see Table 5.2) to changes of strength properties of the fault zones as long as no ice lake is present.

3) With the presence of an ice lake, the models show minor sensitivity (27.1% to 19.8%, see Table 5.2) to changes in fault zone strength from minimum to mean values. There is a large difference in model response when the strength increases from mean to maximum values.

If all the existing fault zones are modelled with the same high stiffness, the following results are obtained for the low stress case and the minimum fault zone strength for the first loading step (3 km ice) with and without ice lake.

- A model with uniform stiffness and minimum fault zone strength, without the ice lake, does not fail at all. In addition, the shear deformation and the stress anomaly in the vicinity of Fault Zone 2 diminishes.

- The same model as above, simulating an ice lake, shows even more failure compared to the case when Fault Zones 2 and 14 have less stiffnesses. The additional failure takes place in Fault Zone 2, and its intersection with Fault Zones 4, 5 and 6, which have failed throughout the model with shear displacements around 0.5 m. The stress anomalies are similar to the non-uniform stiffness case with the major anomalies located at the bottom of the model.

This additional result suggests that the model is also sensitive to the stiffness assumed for the fault zones.

An analytical strength/stress ratio, F, defined by Eq.(4) in Appendix 1, is plotted versus depth in Figure 5.12 for Fault Zone 5 for the low stress state during load step I (3 km ice). Fault Zone 5 was chosen due to its position close to the location for a repository, recommended by Rosengren and Stephansson, (1990)

For the minimum fault zone strength, the introduction of the ice lake causes the curve to drop below F=1 from approximately 200 m depth down to the model base. Similar results are obtained from the UDEC analyses when comparing Figures 5.10a and 5.11a.

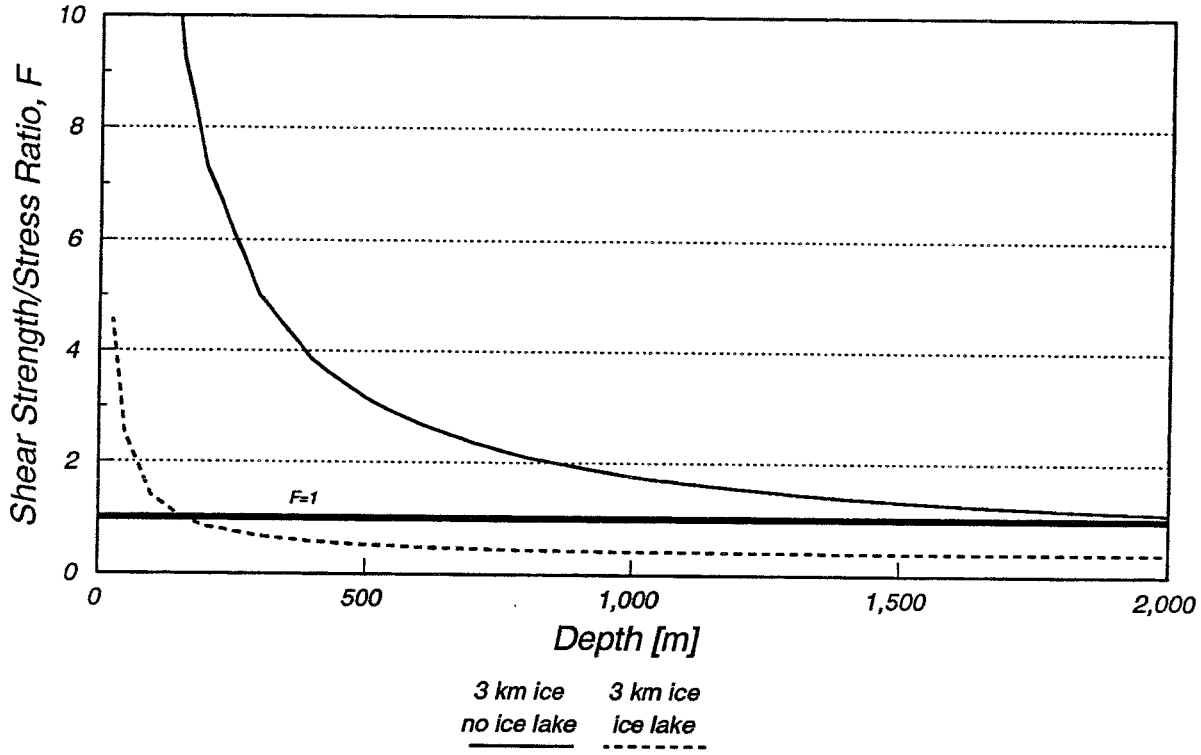

Figure 5.12 Analytically calculated shear strength/stress ratios for Fault Zone 5 versus depth using minimum shear strength properties.

Figure 5.13 shows the analytically calculated strength/stress ratios versus depth for Fault Zone 5 for the three fault zone strengths. The figure represents loading step I (3 km ice), including the ice lake. The three strength cases (minimum, mean and maximum) are plotted versus depth. The diagram shows that Fault Zone 5 with mean strength fails less (from approximately 1300 m depth) than with minimum strength. The maximum strength curve however, is above F=1 throughout the model. This can also be seen in the UDEC results presented in Figure 5.11. The difference in failure when increasing the strength from mean to maximum is obvious.

The relatively insensitive response to changes in fault zone strength properties for models with no ice lake is due to the fact that the induced shear deformations in fault zones are within the elastic range. The failures appear to be caused by the differences in fault zone stiffness rather than the assumed fault zone strengths.

Note that the analytical solution only represents peak shear strength and does not account for the loss of strength due to the constitutive model used in UDEC, in which the cohesion is eliminated when the shear strength is reached. It also does not include propagation of failures or stress redistribution.

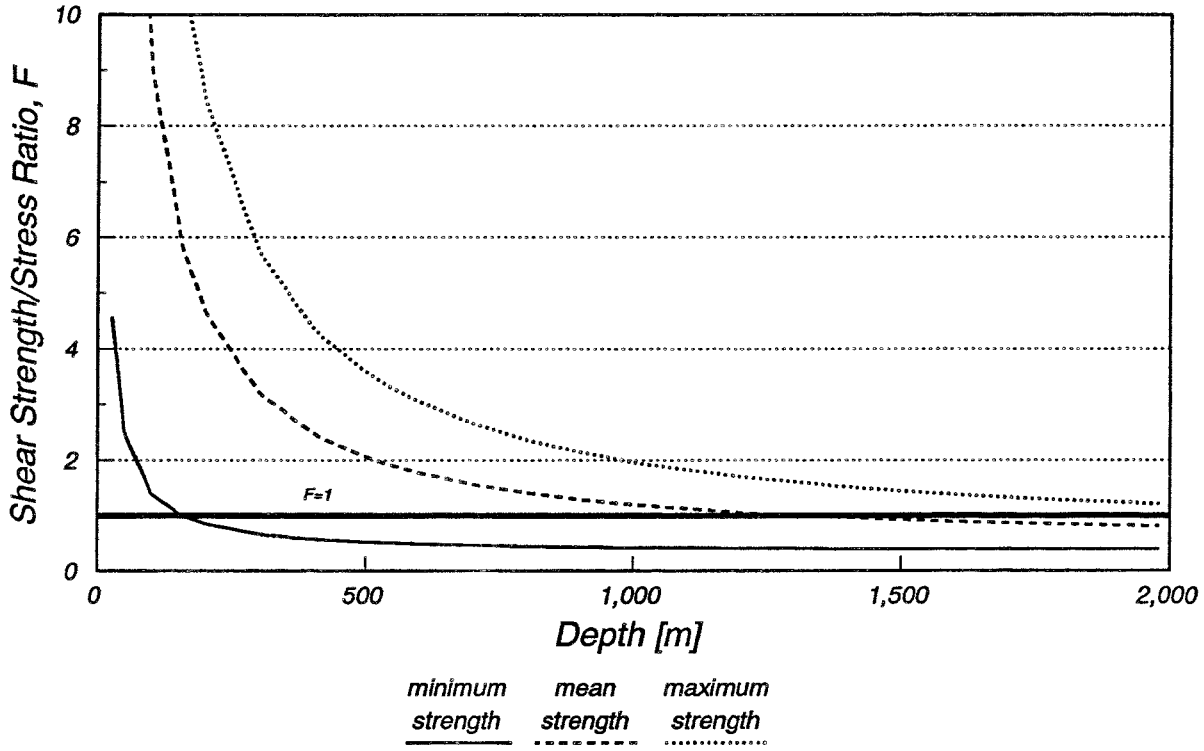

Figure 5.13 Analytically calculated shear strength/stress ratios for different strength cases. Loading step I (3 km ice) and ice lake.

This explains, to some extent, the differences between the results of the analytical solution and the numerical model. This can be seen when comparing the strength/stress curve for the minimum and the mean fault zone strength in Figure 5.13 with the failure plots for the same strength cases in Figure 5.11. Figure 5.13 indicates that Fault Zone 5 should fail over almost the whole depth for the minimum fault zone strength and the mean should only fail over the deepest 700 m. However, Figure 5.11 shows that Fault Zone 5 with mean strength fails almost as much as with minimum strength.

5.3 MEDIUM IN-SITU STRESS STATE

The medium in-situ stress was applied to model No's. 4, 5, 6, 13, 14 and 15, of which No. 13, 14 and 15 simulate the pore pressure from the ice lake. This in-situ stress state is the same as the stress state used in the previous analysis by Rosengren and Stephansson (op. cit.). The stress state results in an hydrostatic stress condition at a depth of approximately 940 m. By adding 3 km of ice load to the model, the hydrostatic stress conditions is transferred to a depth of approximately 300 m.

5.3.1 Stress

Major stress anomalies occur in the vicinity of Fault Zones 2 and 14 during loading step I (3 km ice), for the case of no ice lake. The anomalies are not affected by increasing fault zone strength. They are, however, reduced for the subsequent loading steps (1 km ice and the ice wedge). The final stress field for loading step IV (no load) appears to be equal to the initial (in-situ) stress state.

Figure 5.14 shows the principal and shear stresses (σ_{xy}) versus depth for the profile at x=-540 m and x=175 m. The results demonstrate that increasing fault zone strength has no effect on the stress distribution along the two profiles.

The effect from introducing an ice lake can be seen for loading step I (3 km ice) in Figure 5.15 . The stress anomalies that occurred in models without the ice lake have diminished. No differences in stress distribution along the two stress profiles can be seen when increasing the fault zone strength.

It can be concluded that the stress field in the models is sensitive to the introduction of an ice lake and insensitive to changes in the fault zone strength.

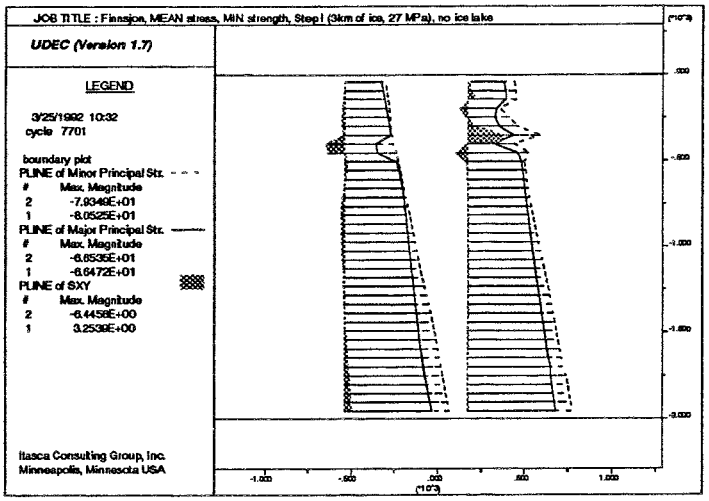

a)

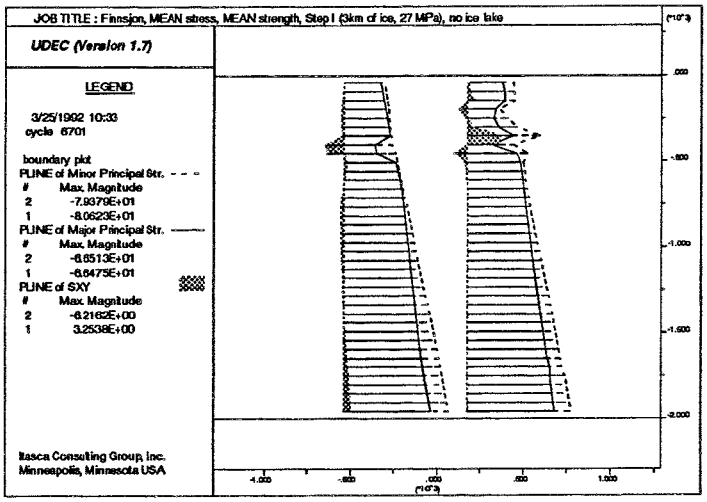

b)

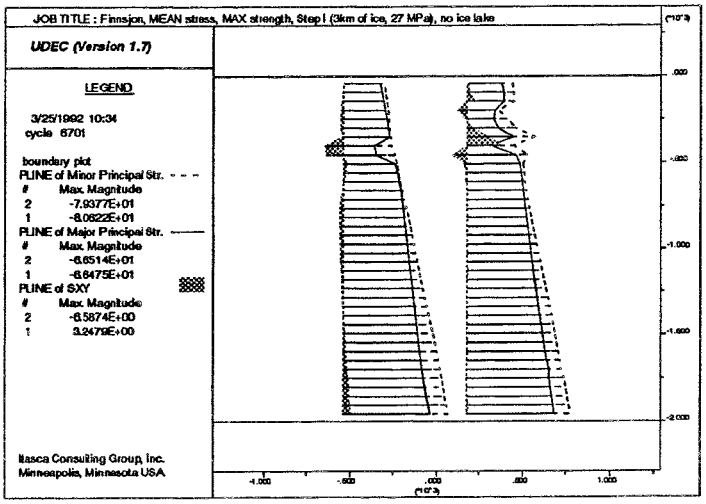

c)

Figure 5.14 Principal stresses and shear stress (σxy) versus depth without ice lake and low stress state, loading step I. a) minimum (Model 4), b) mean (Model 5) and, c) maximum (Model 6) strength of fault zones.

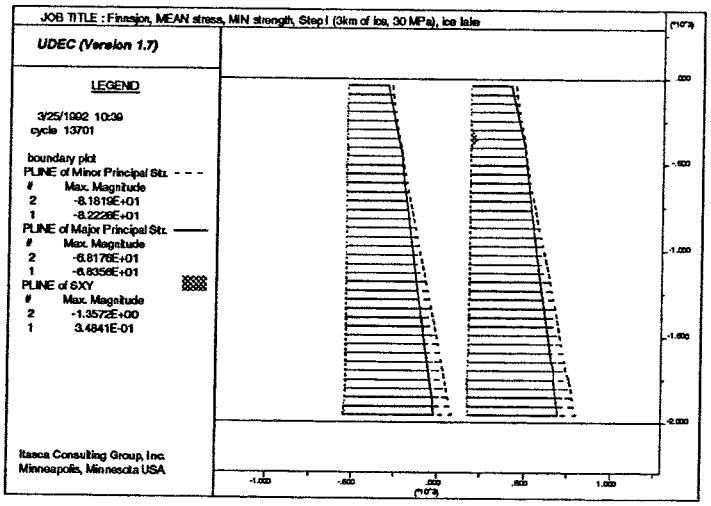

a)

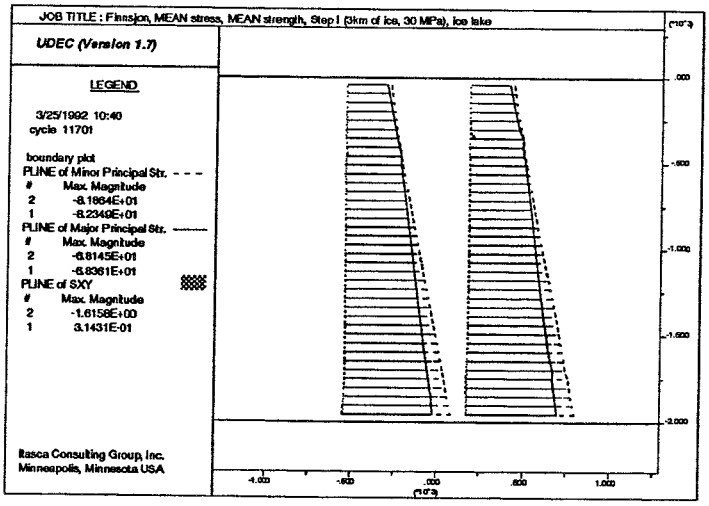

b)

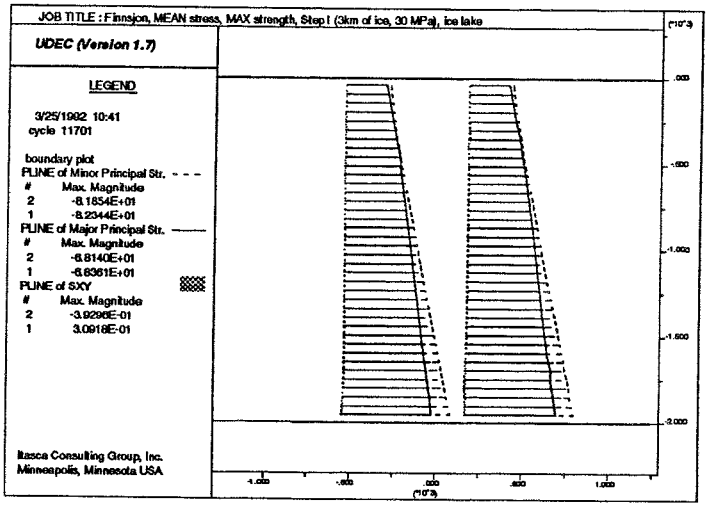

c)

Figure 5.15 Principal stresses and shear stress (σxy) versus depth with ice lake and low stress state, loading step I. a) minimum (Model 13), b) mean (Model 14) and, c) maximum (Model 15) strenght of fault zones.

5.3.2 Shear Displacement on Fault Zones

Models 4, 5 and 6 (without the ice lake) show shear displacements on fault zones similar to those in the low stress case - i.e., mainly elastic deformation of Fault Zones 2, 4, 6, 12, and 14 (Figures 5.9 and 5.16). The maximum shear displacement for loading step I (3 km ice) is about 4.6 cm for all three strength cases. Some inelastic deformations occur in Fault Zones 6 and 12 which increase during the subsequent loading steps (1 km ice and the ice wedge). A slight effect of the increased strength properties can be noticed for loading step II and III (1 km ice and the ice wedge). This suggests that the shear displacements on fault zones are relatively insensitive to strength properties for this stress state and no ice lake.

When introducing the ice lake, the elastic shear displacements diminish in Fault Zones 2, 12 and 14 for loading step I (3 km ice). However, in the upper part of the model, some inelastic shear deformation occurs in Fault Zones 2, 4 and 5 for loading step I (3 km ice). For the subsequent loading steps (1 km ice and the ice wedge), some additional inelastic shearing occurs for the minimum strength case in Fault Zones 6 and 12. The maximum shear displacement magnitude amounts to approximately 8.5 cm for loading step III (ice wedge), which means that the maximum magnitude is twice the magnitude of the no ice lake case (Figure 5.17).

By increasing the fault zone strength from minimum to maximum strength, the shear displacements on fault zones decrease to 0.9 cm in loading step III (ice wedge). This means that the ice lake case is more sensitive to changes of strength properties than the case without the ice lake. However, the sensitivity is not pronounced within the range of properties modelled.

Based on the results, it can be concluded that the shear displacements on fault zones are sensitive to the introduction of an ice lake. For the case without the ice lake, the model is insensitive to changes of fault zone strength properties, whereas the ice lake case shows sensitivity when going from minimum to maximum fault zone strength.

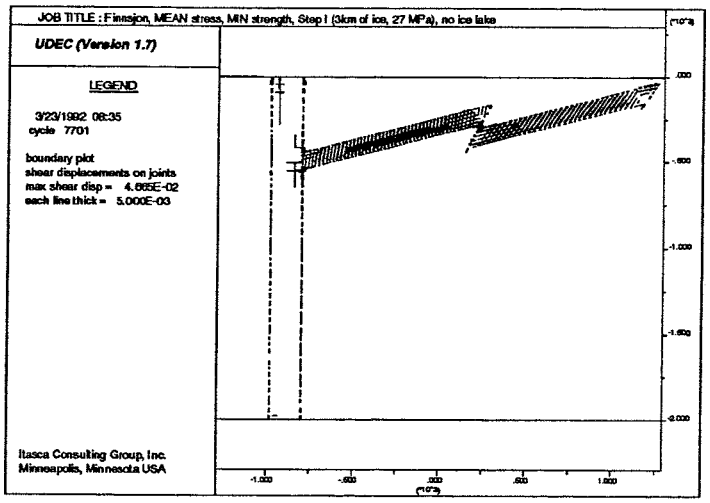

a)

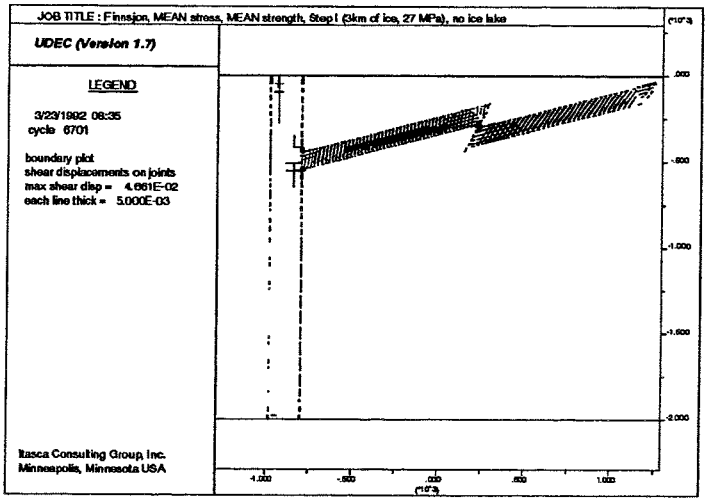

b)

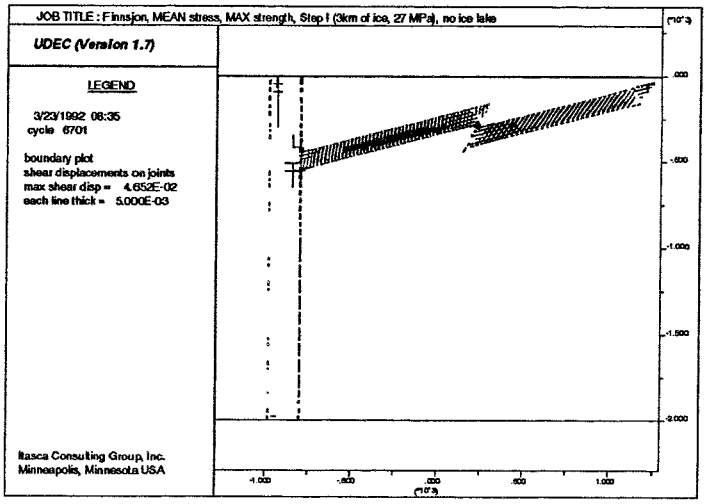

c)

Figure 5.16 Shear displacement on fault zones for medium in-situ stress and no ice lake, loading step I (3 km ice). a) minimum (Model 4), b) mean (Model 5) and c) maximum (Model 6) fault zone strength.

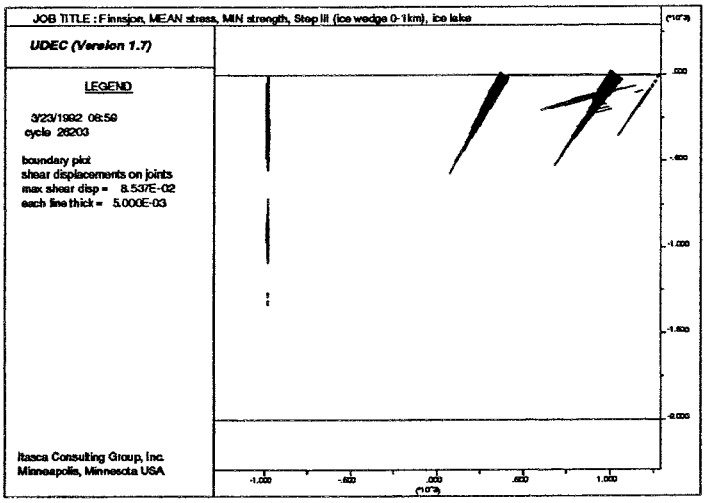

a)

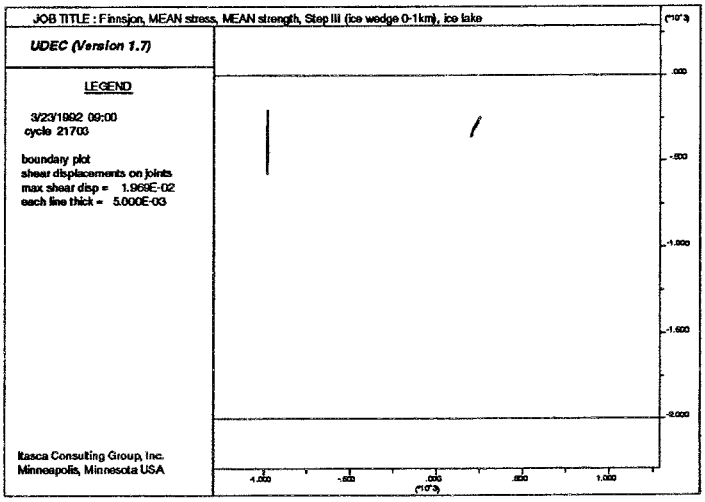

b)

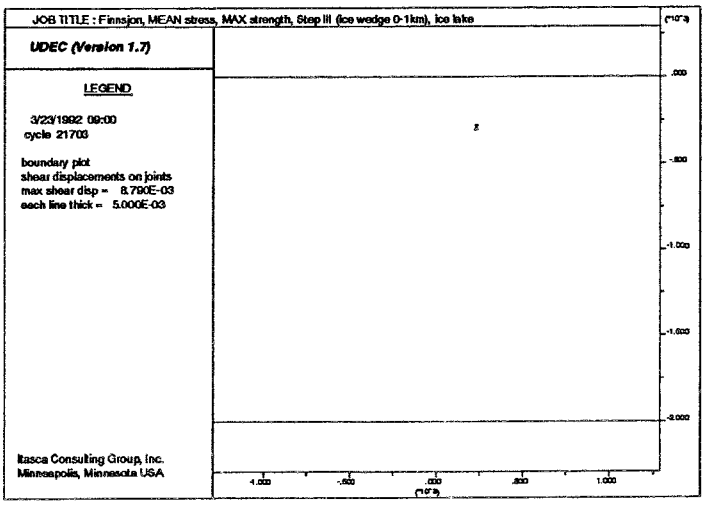

c)

Figure 5.17 Relative shear displacement on joints for medium in-situ stress and ice lake, loading step III (ice wedge). a) minimum (Model 13), b) mean (Model 14) and c) maximum (Model 15) fault zone strength.

5.3.3 Failure of Fault Zones

For the cases without the ice lake, the amount of failure of fault zones increases from approximately 3% for the first loading step (3 km ice) to more than 6% after the complete loading sequence for the minimum strength case. This increase in failure only appears for the minimum strength case. By increasing the strength properties of the fault zones, a gradual reduction of failed fault zones is obtained, as shown in Figure 5.18. Almost no additional failure occurs for the subsequent loading steps when using the mean and the maximum fault zone strength.

By adding the pore pressure from the ice lake, some additional failure occurs for the minimum strength case. The mean and the maximum strength cases are not affected by the increased pore pressure (Figure 5.19). For the minimum strength case, the amount of fault zone failures increases for the subsequent loading steps (1 km ice, ice wedge).

The most pronounced reaction can be seen for the minimum strength case when introducing the ice lake. Otherwise, this stress case is insensitive to changes of fault zone properties - i.e., the model shows similar failure pattern with and without the ice lake for the mean and the maximum strength cases.

Table 5.3 shows the failure in percent of total fault zone length for each strength and pore pressure (i.e., ice lake/no ice lake) for loading step IV (no load).

Table 5.3 Percentage of failed fault zone length compared to total fault zone length for the medium stress state, (loading step IV, no load)

Strength of fault zones	Model No.	No ice lake	Model No.	Ice lake
Minimum	4	6.2 %	13	8.2 %
Mean	5	1.8 %	14	1.7 %
Maximum	6	0.4 %	15	0.4 %

As can be seen from Table 5.3, the model is sensitive to the introduction of an ice lake for the minimum strength case and also to changes of fault zone strength properties both with and without the ice lake.

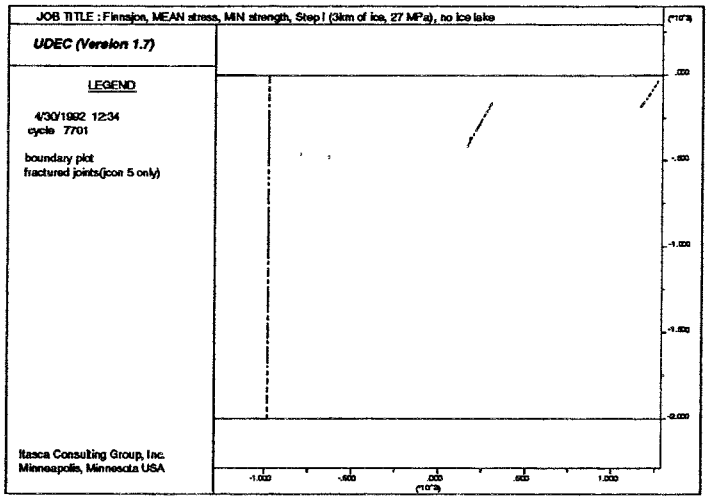

a)

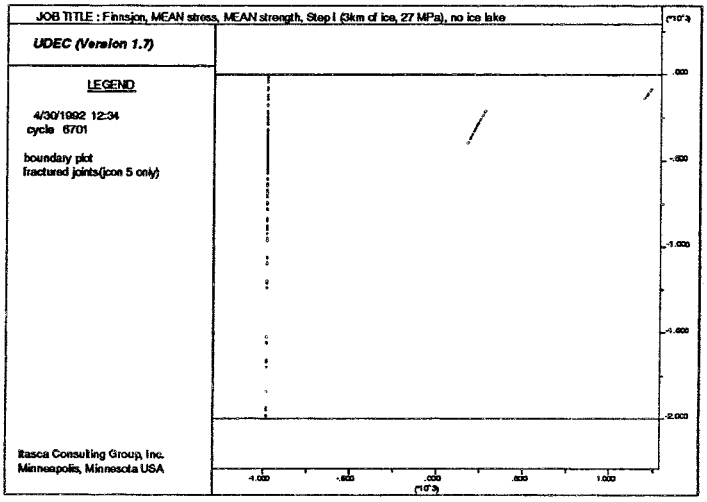

b)

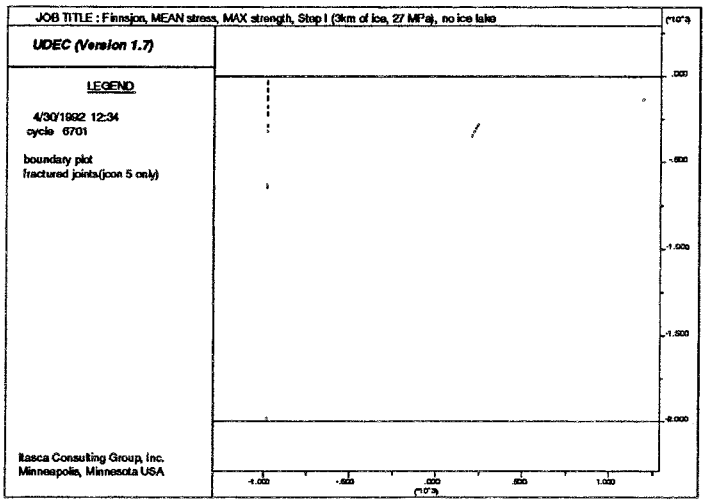

c)

Figure 5.18 Fractured fault zones for loading step I (3 km ice) with medium in-situ stress and no ice lake. a) minimum (Model 4), b) mean (Model 5) and c) maximum (Model 6) fault zone strength.

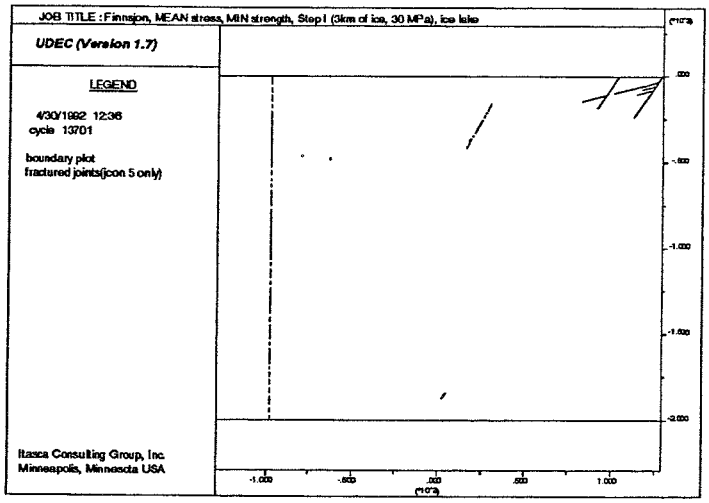

a)

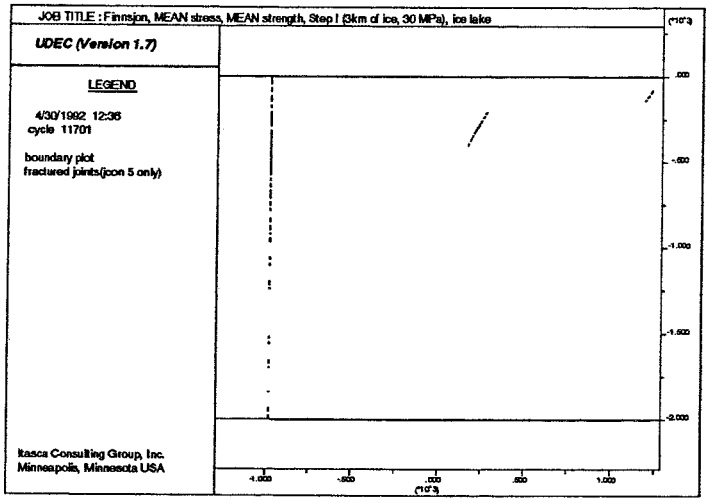

b)

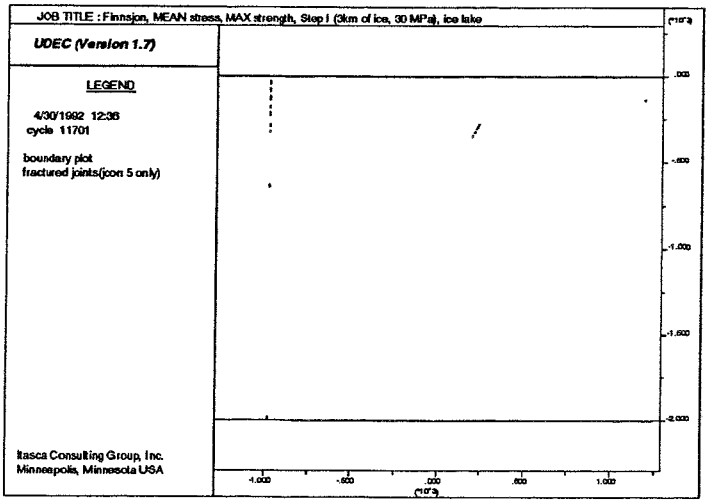

c)

Figure 5.19 Fractured fault zones for loading step I (3 km ice) with medium in-situ stress and ice lake. a) minimum (Model 13), b) mean (Model 14) and c) maximum (Model 15) fault zone strength.

5.3.4 Discussion and Conclusions

Based on the results presented previously, the following general conclusions can be drawn from modelling the medium state of stress.

1) The models are somewhat sensitive to the introduction of an ice lake. The sensitivity, however, is not pronounced.

2) The models show minor sensitivity to fault zone strength properties for the cases without the ice lake.

3) For the cases with an ice lake, the model is sensitive to fault zone strength in terms of fault zone failures and shear displacements on fault zones.

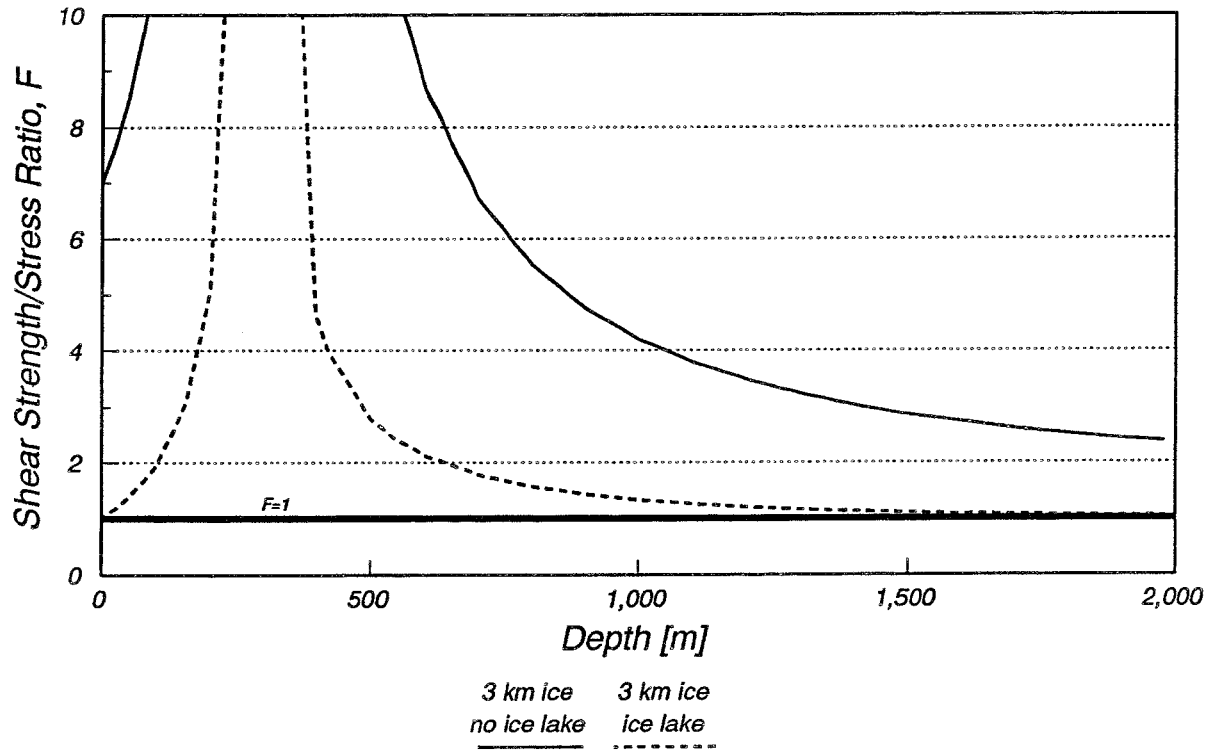

Figure 5.20 Analytically calculated shear strength/stress ratios for Fault Zone 5 versus depth using minimum shear strength properties and medium in-situ stress state.

The introduction of an ice lake causes the analytically calculated strength/stress ratio for Fault Zone 5 to more or less coincide with F=1 near the ground surface and at depth, whereas the no ice lake strength/stress ratio is well above F=1 for the minimum strength case, as shown in Figure 5.20. This explains the results shown in Figures 5.18a and 5.19a in which Fault Zone 5 (and the parallel Fault Zone 4) fail near the ground surface and at depth when the ice lake is modelled together with the minimum fault zone strength.

The peak in the strength/stress ratio at approximately 300 m depth is due to the hydrostatic stress state at this depth.

The failure, occurring in the models with no ice lake, is probably caused mostly by differences in fault zone stiffness. Therefore, it can not be explained by the analytical solution.

By varying the fault zone strength, it appears analytically that the minimum strength is the only case close to F=1 when modelling the ice lake (Figure 5.21). This explains why the only numerically modelled strength case showing additional failures from the increased pore pressure is the one with minimum fault zone strength, as seen in Figure 5.19.

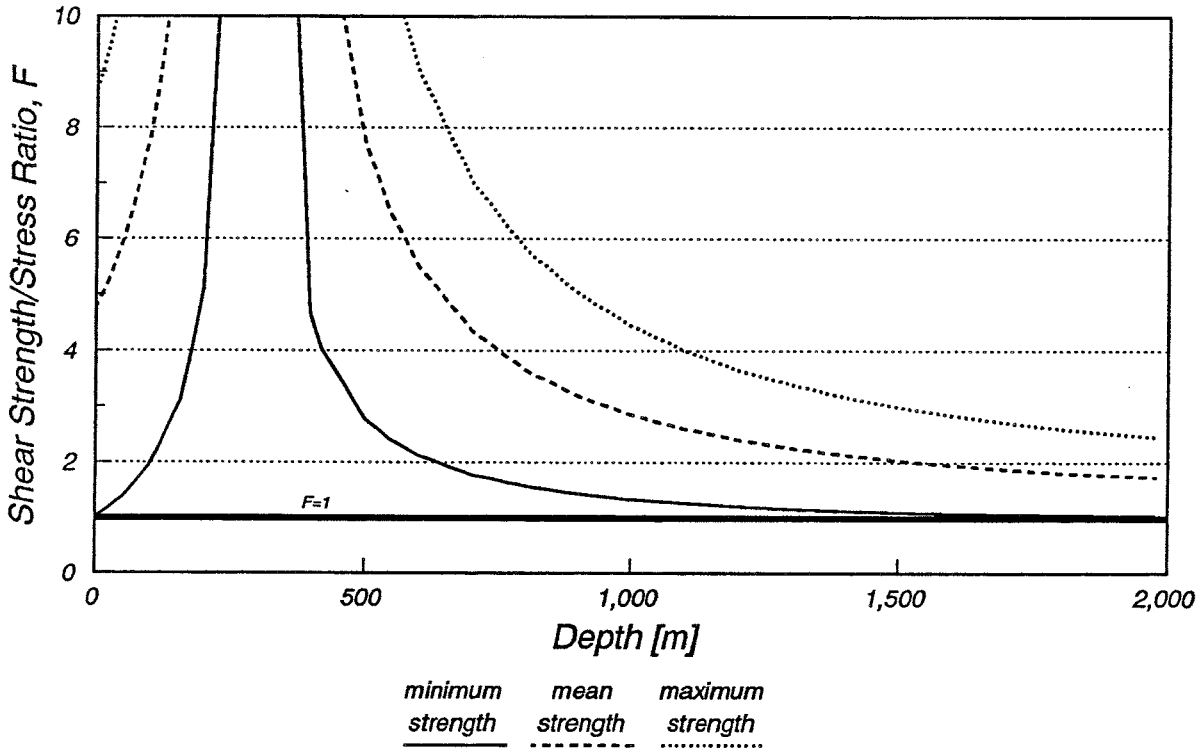

Figure 5.21 Analytically calculated shear strength/stress ratios for different strength cases. Loading step I (3 km ice), ice lake and medium in-situ stress state.

The reason that the stress anomalies diminish when introducing an ice lake is that the increased pore pressure in the fault zones more or less equilibrate the ice load. Since the shear displacements on joints in Zone 2 are within elastic ranges, even for the minimum strength case, no differences in shear displacements can be seen between the different strength cases.

5.4 HIGH IN-SITU STRESS STATE

The high stress state was applied to model No's 7, 8, 9, 16, 17 and 18, of which No. 16, 17 and 18 simulated the load from the ice lake. The maximum stress state is characterized by a high horizontal stress at zero depth and a high stress gradient, which makes the maximum principal stress horizontal regardless of depth. When adding 3 km of ice overload, the stresses became hydrostatic at a depth of approximately 1500 m.

5.4.1 Stress

Major stress anomalies occur in the vicinity of Fault Zones 2 and 14 for the case of no ice lake, loading step I (3 km ice). No effects on the stress anomalies can be seen by increasing the fault zone strength (Figure 5.22). The stress anomalies diminish however for the subsequent loading steps.

When introducing the ice lake, the stress anomalies diminish, as can be seen from the two stress profiles in Figure 5.23.

The stress field is sensitive to the introduction of an ice lake but insensitive to strength properties of the fault zone, regardless of ice lake presence.

5.4.2 Shear Displacement on Fault Zones

For the case of no ice lake, the shear displacements on joints show a similar trend as the low and medium stress cases. They are concentrated to Fault Zones 2 and 14 and appear to be mainly elastic, uniformly distributed shear deformations with maximum magnitudes of 4.6 cm in loading step I (3 km ice). The increase of fault zone strength does not affect the pattern of displacement or the maximum magnitudes (Figure 5.24). A gradual reduction of shear deformation occurs in the subsequent loading steps, and the maximum magnitude for the minimum strength case is 1.2 cm for the ice wedge load (loading step III).

Subjecting the model to ice lake pore pressure, the shear displacements described above diminish and, for the minimum strength case, Fault Zone 2 shows shear displacements which increase in loading step II (1 km ice) to approximately 3 cm (Figure 5.25).

By increasing the fault zone strength, the shear displacements on the fault zones are reduced to be almost zero for the maximum fault zone strength.

The models are sensitive to the ice lake loading. The no ice lake cases are insensitive to variations in fault zone strength properties.

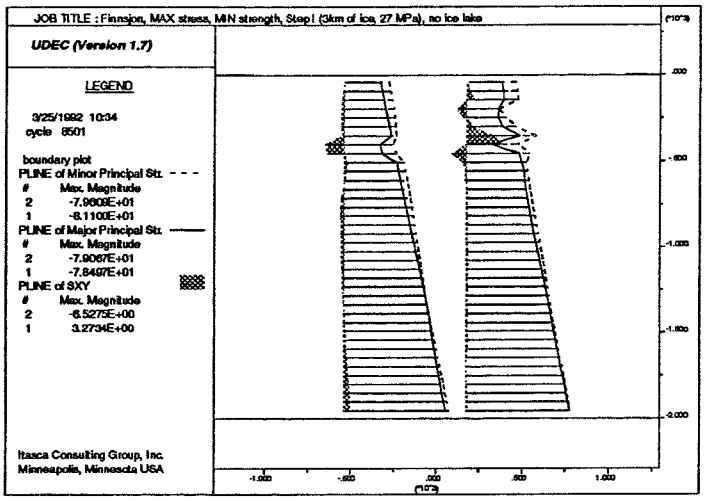

a)

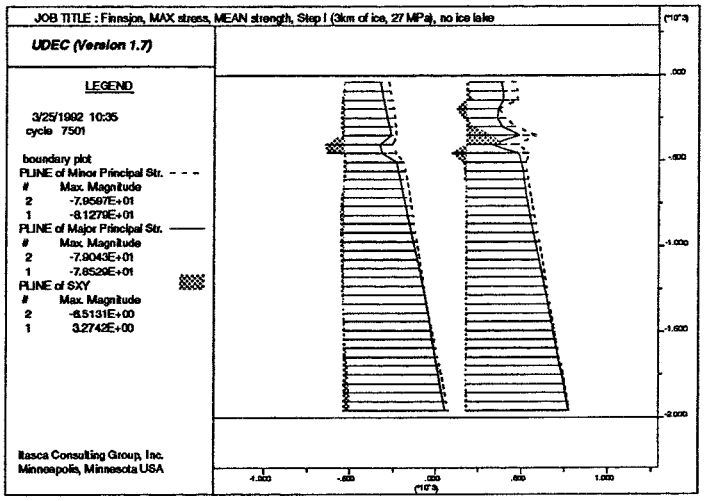

b)

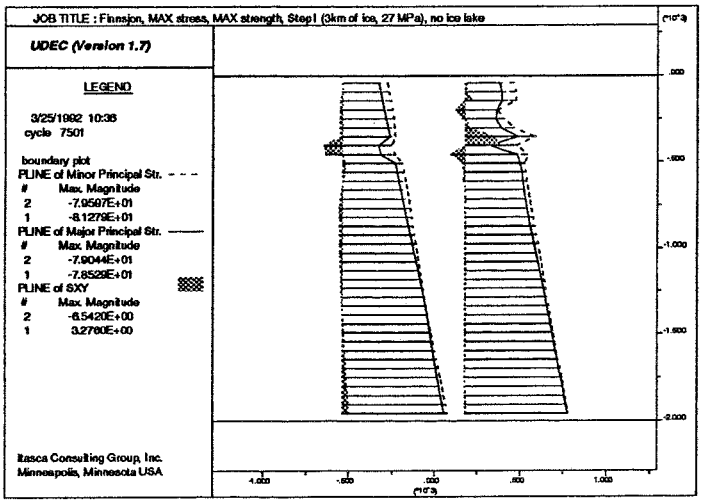

c)

Figure 5.22 Principal stresses and shear stress (σxy) versus depth for high in-situ stress state without ice lake, loading step I. a) minimum (Model 7), b) mean (Model 8) and, c) maximum (Model 9) strength of fault zones.

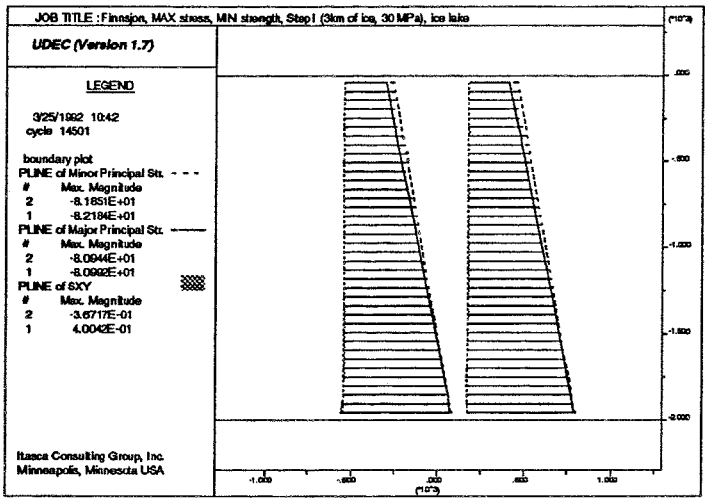

a)

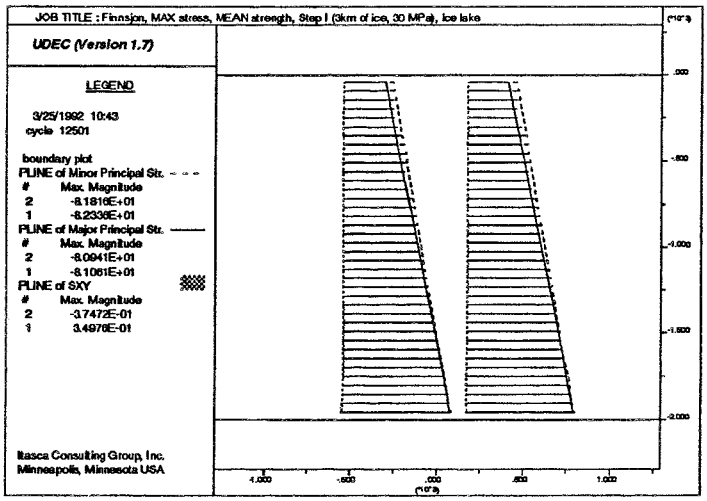

b)

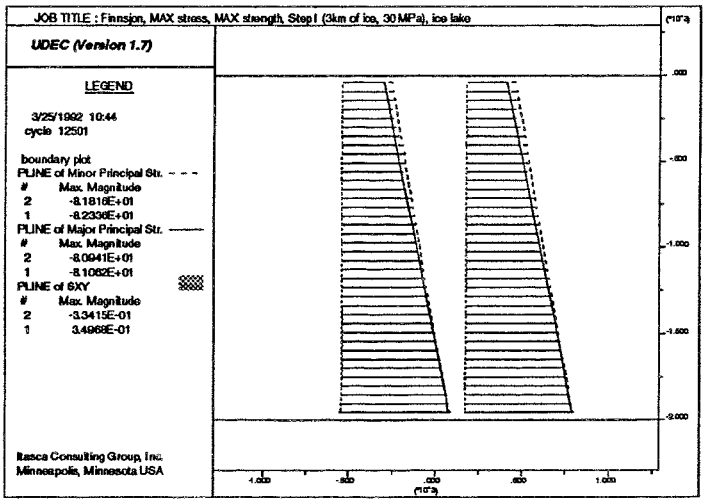

c)

Figure 5.23 Principal stresses and shear stress (σxy) versus depth for high in-situ stress state with ice lake, loading step I. a) minimum (Model 16), b) mean (Model 17) and, c) maximum (Model 18) strength of fault zones.

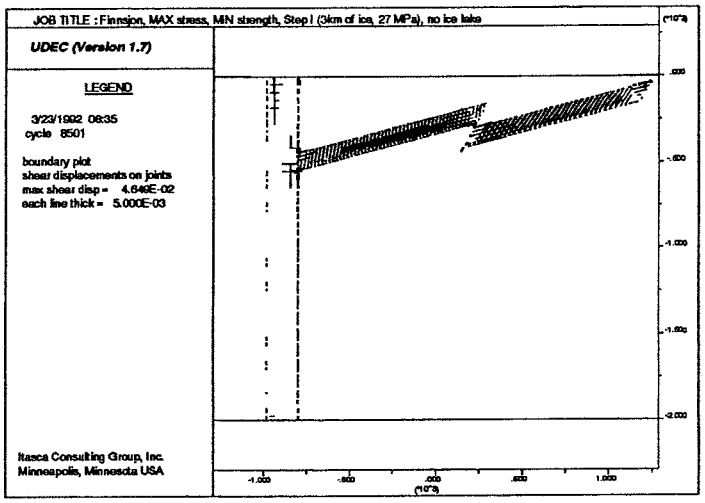

a)

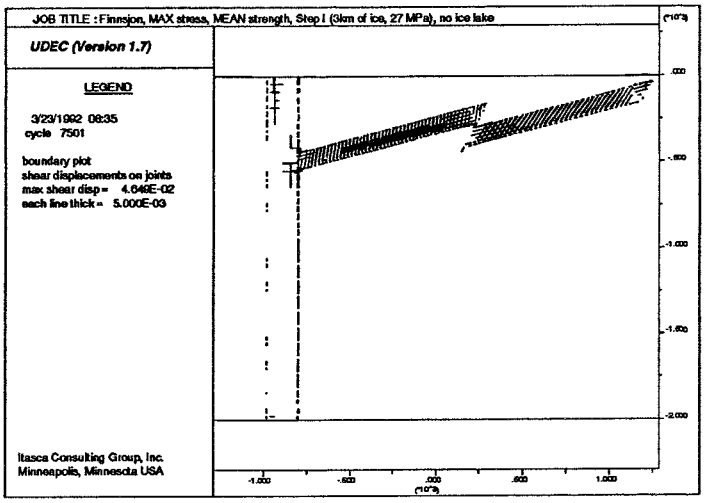

b)

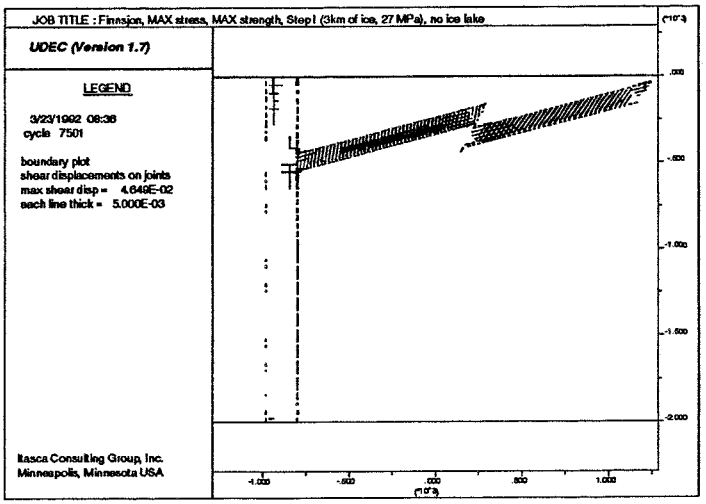

c)

Figure 5.24 Shear displacement on fault zones for high in-situ stress and no ice lake, loading step I (3 km ice). a) minimum (Model 7), b) mean (Model 8) and c) maximum (Model 9) fault zone strength.

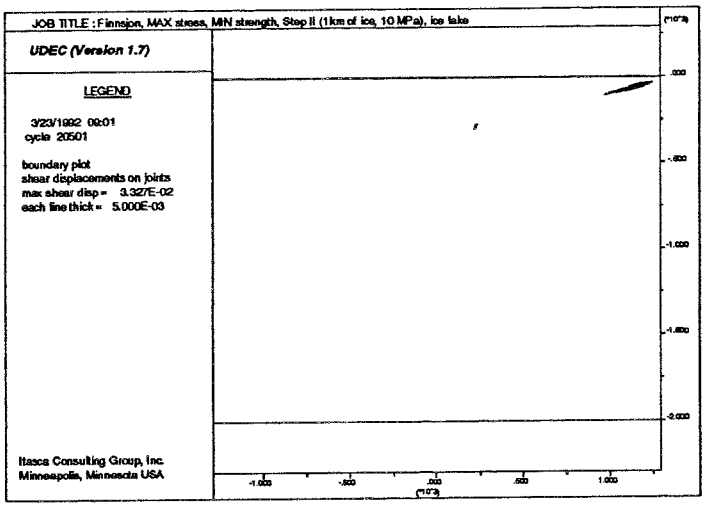

a)

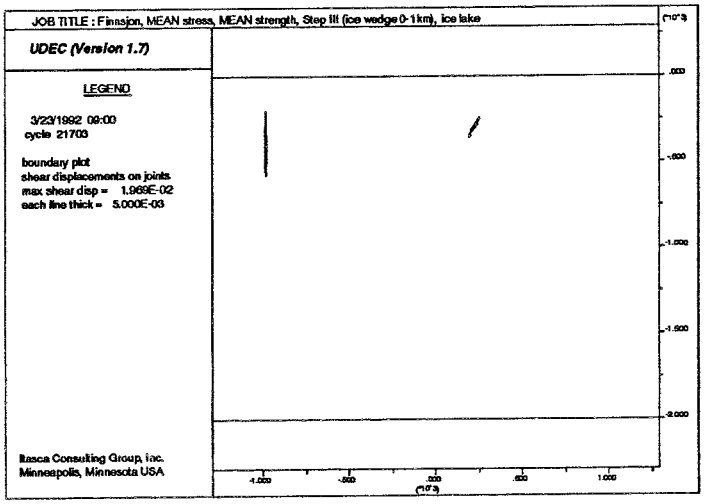

b)

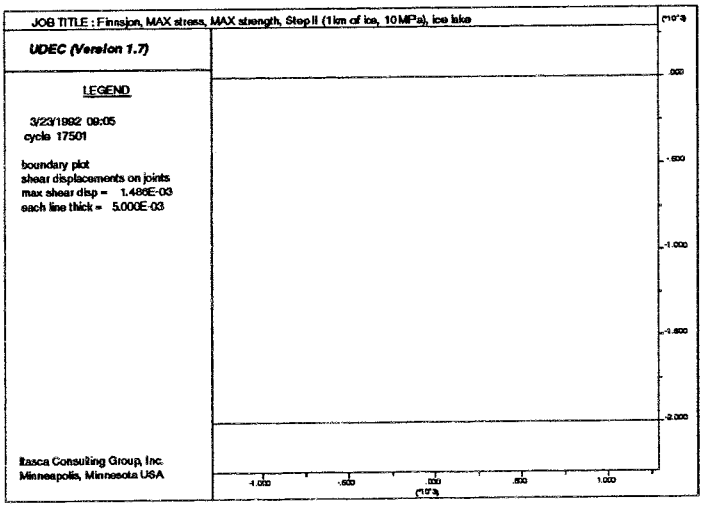

c)

Figure 5.25 Relative shear displacement on joints for high in-situ stress and ice lake, loading step III (ice wedge). a) minimum (Model 16), b) mean (Model 17) and c) maximum (Model 18) fault zone strength.

5.4.3 Failure of Fault Zones

For the case of no ice lake, all failure of fault zones occurs during the first loading step (3 km ice). However, a very small amount of fault zones fails from the overload. By increasing the fault zone strength from minimum to mean strength, the failure is completely eliminated (Figure 5.26).

When adding the ice lake, some minor, additional failure occur near the ground surface in Fault Zone 2 for the minimum strength case. A small increase in fault zone failure occur during loading step II (1 km ice).

Still, the length of failed fault zones is very small (see Table 5.4). By increasing the fault zone strength, the amount of failed fault zones diminish (see Figures 5.26 and 5.27).

Table 5.4 Percent failed fault zone length compared to total fault zone length for the high stress state (loading step IV, no load)

Strength of fault zones	Model No.	No ice lake	Model No.	Ice lake
Minimum	7	0.5 %	16	0.8 %
Mean	8	0 %	17	0 %
Maximum	9	0 %	18	0 %

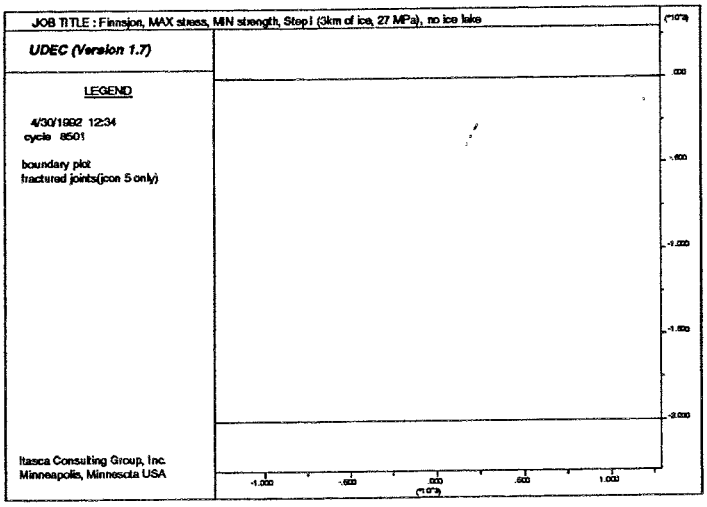

a)

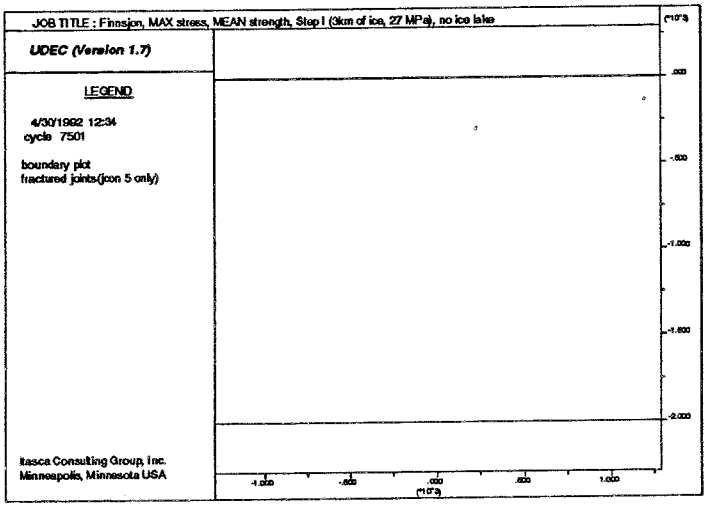

b)

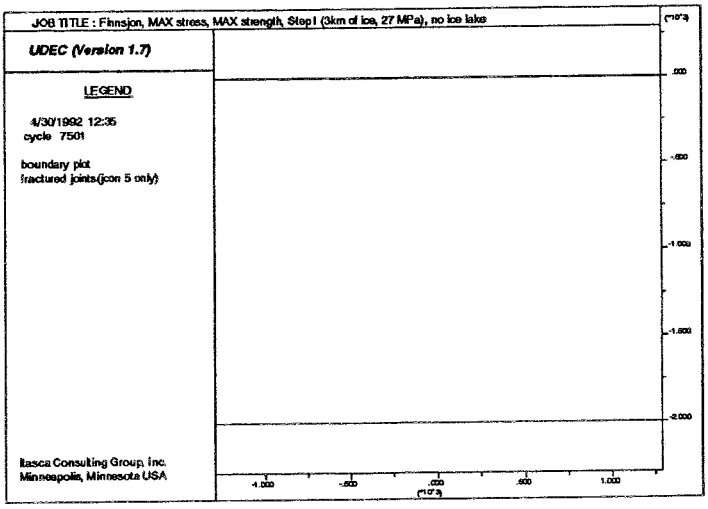

c)

Figure 5.26 Fractured fault zones for loading step I (3 km ice) with high in-situ stress and no ice lake. a) minimum (Model 4), b) mean (Model 5) and c) maximum (Model 6) fault zone strength.

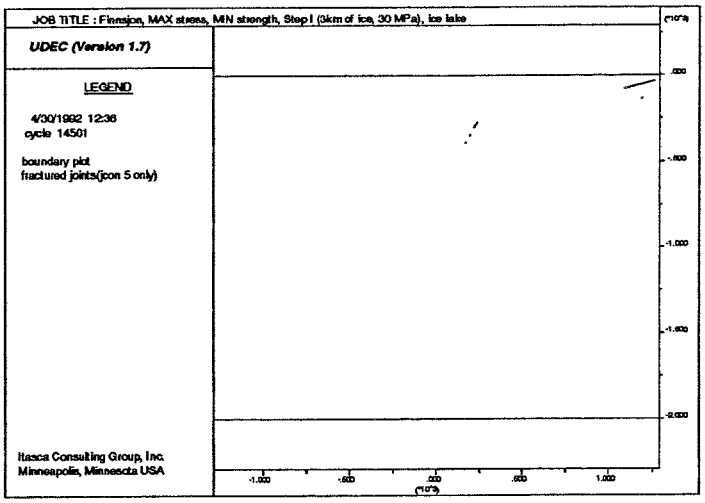

a)

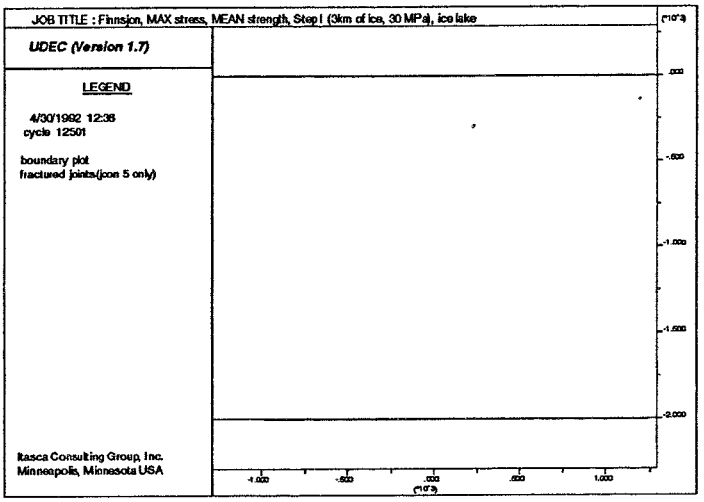

b)

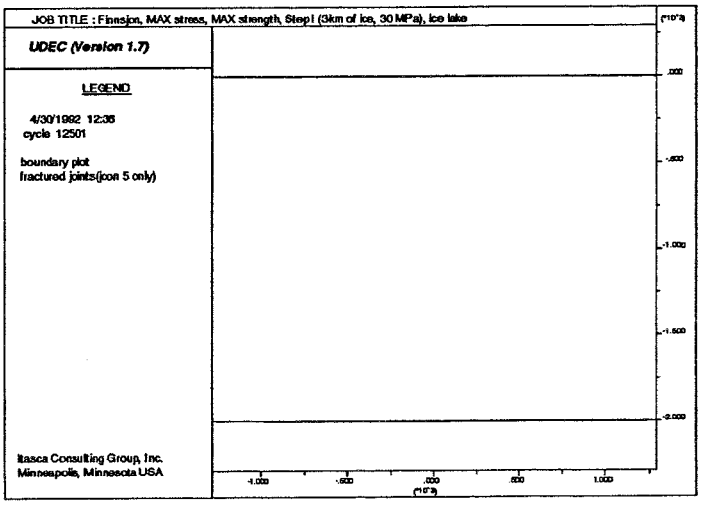

c)

Figure 5.27 Fractured fault zones for loading step I (3 km ice) with high in-situ stress and ice lake. a) minimum (Model 16), b) mean (Model 17) and c) maximum (Model 18) fault zone strength.

5.4.4 Discussion and Conclusions

Based on the results presented previously, the following general conclusions can be drawn from modelling the high stress state.

1) The model is very slightly sensitive to the introduction of an ice lake.

2) The model shows minor sensitivity to fault zone strength properties for both the case of no ice lake and the case of ice lake presence.

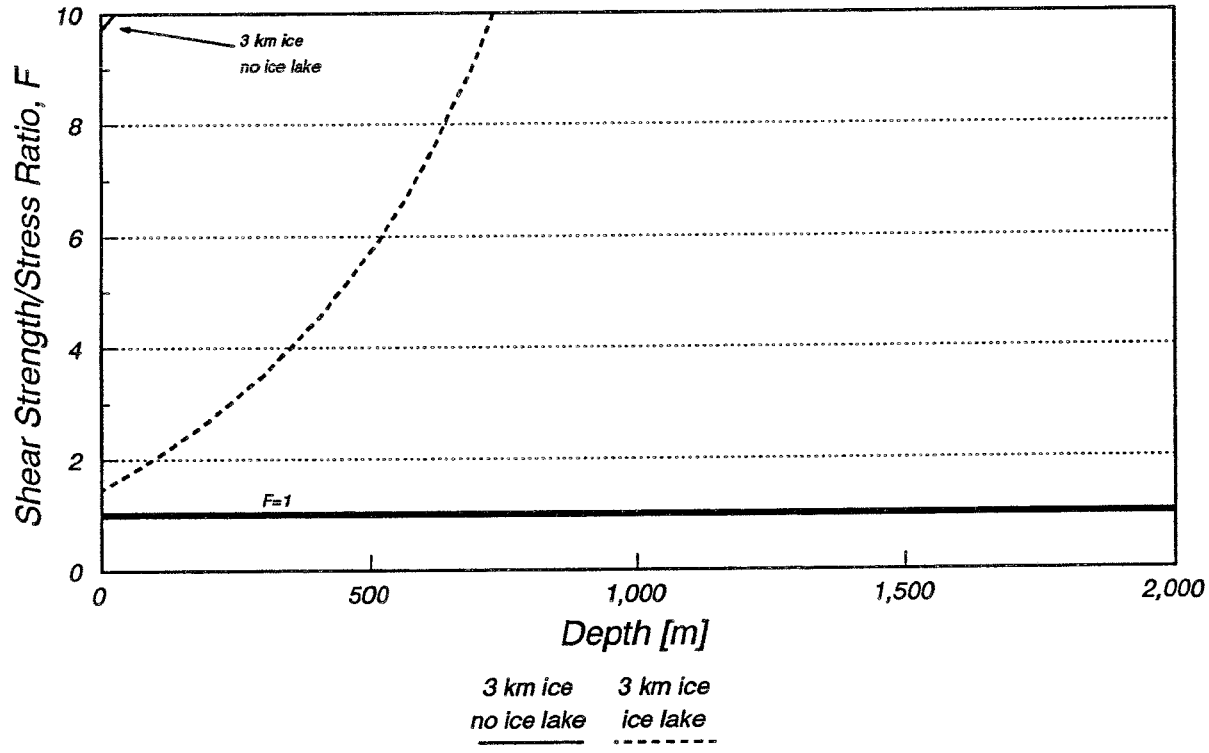

Figure 5.28 Analytically calculated shear strength/stress ratios versus depth using minimum shear strength properties for Fault Zone 5 and high in-situ stress state.

The loading from the ice lake causes the analytically calculated strength/stress ratio, F, to drop to F=1.5 near the ground surface for Fault Zone 5 using the minimum fault zone strength (Figure 5.28). By increasing the strength, the strength/stress ratio is increased to be almost F=8 as the lowest value for the maximum fault zone strength. This is also the result from the model runs shown in Figures 5.26 and 5.27.

The majority of the failures of fault zones is most likely to be caused by stiffness contrasts of the fault zones, as described in section 5.2.4 .

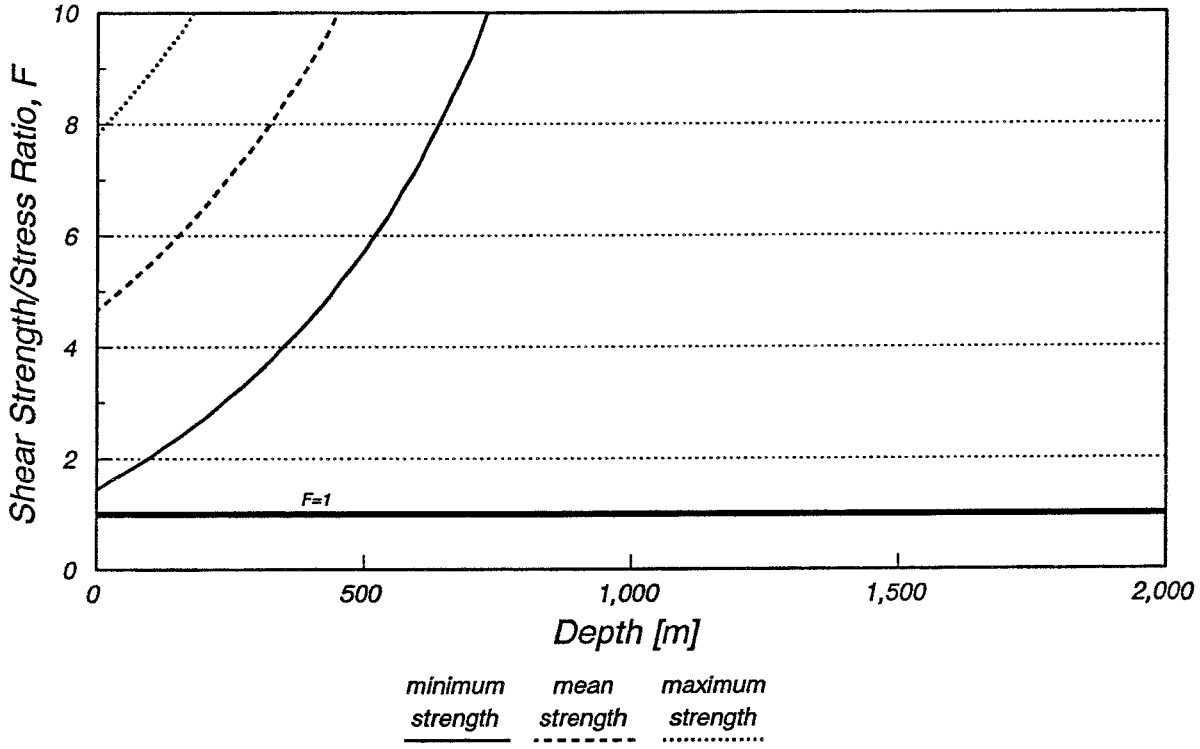

Figure 5.29 Analytically calculated shear strength/stress ratios for different strength cases and high in-situ stress state. Loading step I (3 km ice) and ice lake .

The high in-situ stress state is sensitive to the introduction of an ice lake in terms of stress redistribution in the vicinity of Fault Zones 2 and 14.

The increased fault zone strength has a minor influence on the model - i.e., the model is insensitive to fault zone properties.

6 DISCUSSION

The different in-situ stress states, applied to the models make significant differences in deformation modes and failures. The differences can, to some extent be explained with the analytically calculated strength/stress ratios, which correspond reasonably well with the results from the model runs. The strength/stress curves indicate both the depths of expected failure of fault zones and the sensitivity of the fault zones to changes in strength and/or pore pressure.

As can be seen from these strength/stress ratios, the shape of the curve more or less describes the volume (depth) to be involved in a reduction of F below 1. The more flat and linear the curve is, the larger volume involved in the excess stress region. The shape of the curve depends on the strength properties of the fault zones and the in-situ stress acting in the model. The strength/stress ratio for the three in-situ stress states (low, medium, high) are shown in Figure 6.1 for the case of minimum strength of Fault Zone 5 with 3 km of ice and ice lake. As can be seen, the low in-situ stress state causes the curve to drop below F=1 over a long distance due to its flat character. The medium in-situ stress state makes the curve reach F=1 at the ground surface and at depth, with a rather flat curvature at depth. The high in-situ stress state, however, only makes the curve to approach F=1 at the top of the model.

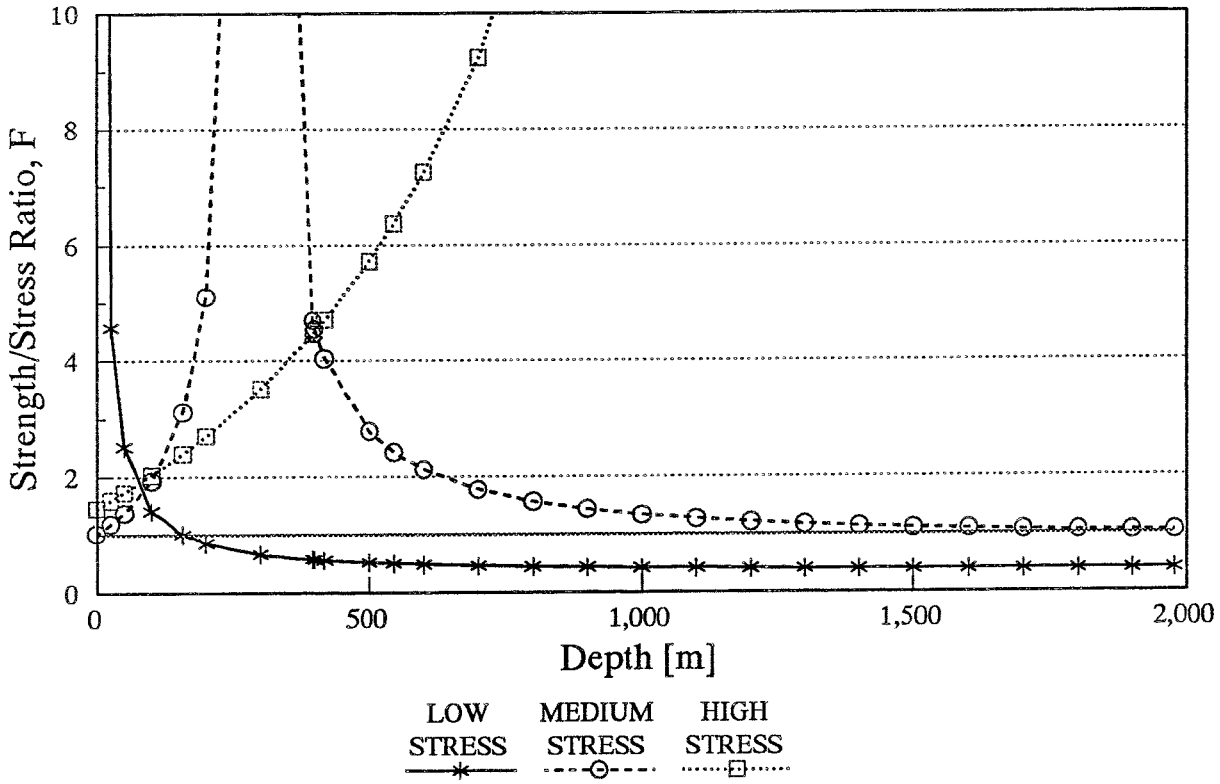

Figure 6.1 Strength/stress ratios of Fault Zone 5 for low, medium and high in-situ stress with 3 km ice and ice lake.

This explains why the low in-situ stress case is the most sensitive to the introduction of the ice lake and to the increase in fault zone strength. It also explains why the medium in-situ stress is the second most sensitive case, and the high in-situ stress was the least sensitive. If the fault zone strength is taken as a criterion to rank the severity of the different stress

states, the high in-situ stress state is the most critical since it requires the highest fault zone strength properties to prevent failure under the in-situ stresses. Consequently, the low in-situ stress state is the intermediate and the medium in-situ stress state is the least critical (see Table 4.2). The differences in normal and shear stiffness of the fault zones causes the stiffer fault zones to fail in most of the cases. A uniform stiffness in the models gives less failure and different shear patterns. The stress anomalies, however, are not affected to any major extent by using equal stiffnesses. The percent of failure of fault zones for all different combinations of in-situ stresses and strengths of fault zones is for loading step I (3 km ice) and loading step IV (no load) presented in Figure 6.2. Almost all failure occurs during the first loading step.

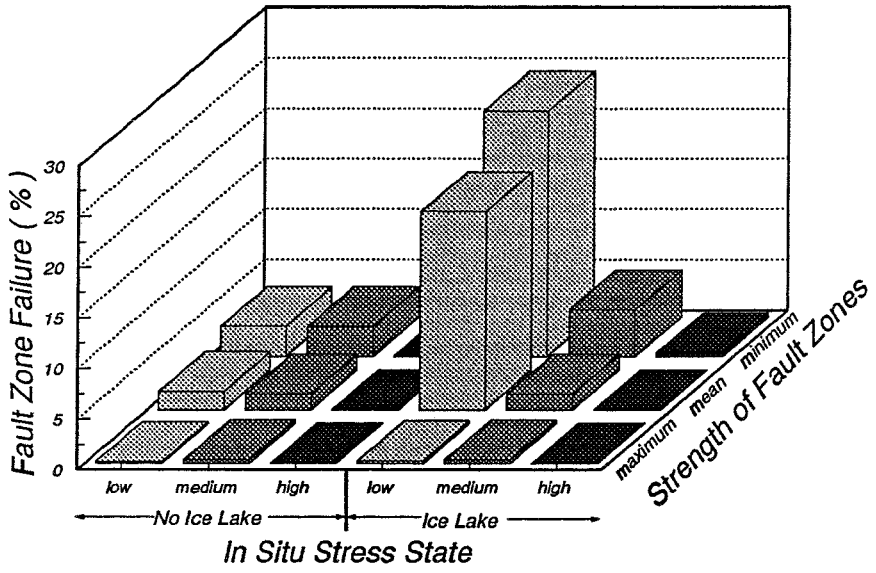

a)

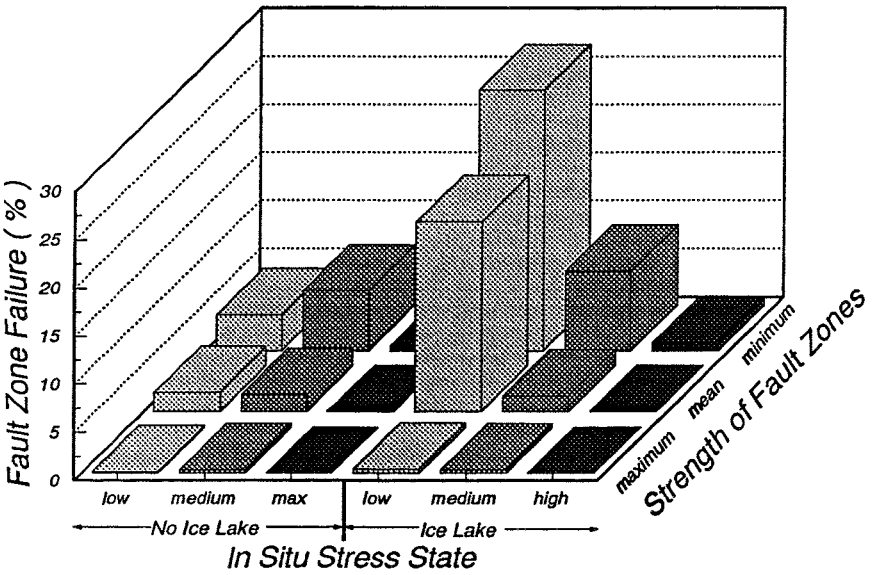

b)

Figure 6.2 Failure of fault zones for all stress / strength combinations analyzed for a) loading step I (3 km ice) and b) loading step IV (no load).

The stress state in the intact rock blocks, acting in the area recommended by Rosengren and Stephansson as suitable for the repository, was compared to the strength of a Stripa granite and a hypothetical rock type, using a Mohr failure criterion. The Stripa Granite was given a cohesion of 25 MPa and a friction angle of 65° [Swan (1978)]. The hypothetical rock type was given a cohesion of 2 MPa and a friction angle of 30° (Figure 6.3). The respective uniaxial compressive strengths, given by eq. (6.1) are 225 MPa and 7 MPa.

$$\sigma_C = \frac{2 \cdot C \cdot \cos\phi}{1 - \sin\phi} \tag{6.1}$$

All in-situ stress cases for 3 km of ice loading were analyzed with and without an ice lake. The results indicate that the strength of most common rocks will not be reached (Figure 6.3). The stress/strength relation presented in Figure 6.4 only considers the effects from the in-situ stresses and the surface loading i.e., no consideration has been taken to the effects from excavating the repository or any thermo-mechanical effects on the near field rock. However, the effect from the major horizontal principal in-sistu stress, σ_H, has not been considered in this analysis since this stress componenet is oriented perpendicular to the plane of analysis.

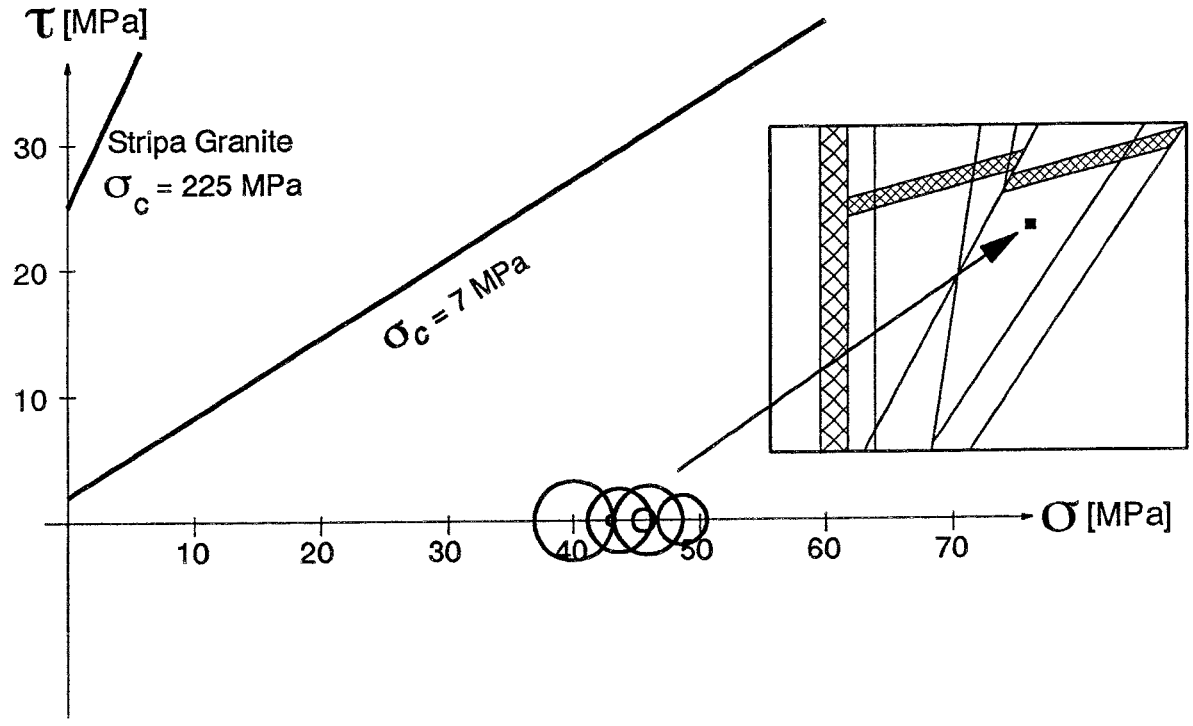

Figure 6.3 Stress states at the recommended location of a repository for all three in-situ stress cases, using 3 km ice load with and without an ice lake. The strength envelopes illustrates the stress/strength relation for two rock types.

The major horizontal principal in-situ stress, σ_H, will increase the deviatoric stresses shown in Figure 6.3. As can be seen in Figure 6.4, the strength requirement (i.e., cohesion and friction angle) to prevent shear failure, in principle changes from (C_1, ϕ_1) to (C_1, ϕ_2) or (C_2, ϕ_1) when using σ_1-σ_3 instead of σ_2-σ_3 as maximum deviatoric stress. However, it is

difficult to speculate about the importance of the major horizontal principal stress component to the shear failure of the intact rock for the Finnsjön area.

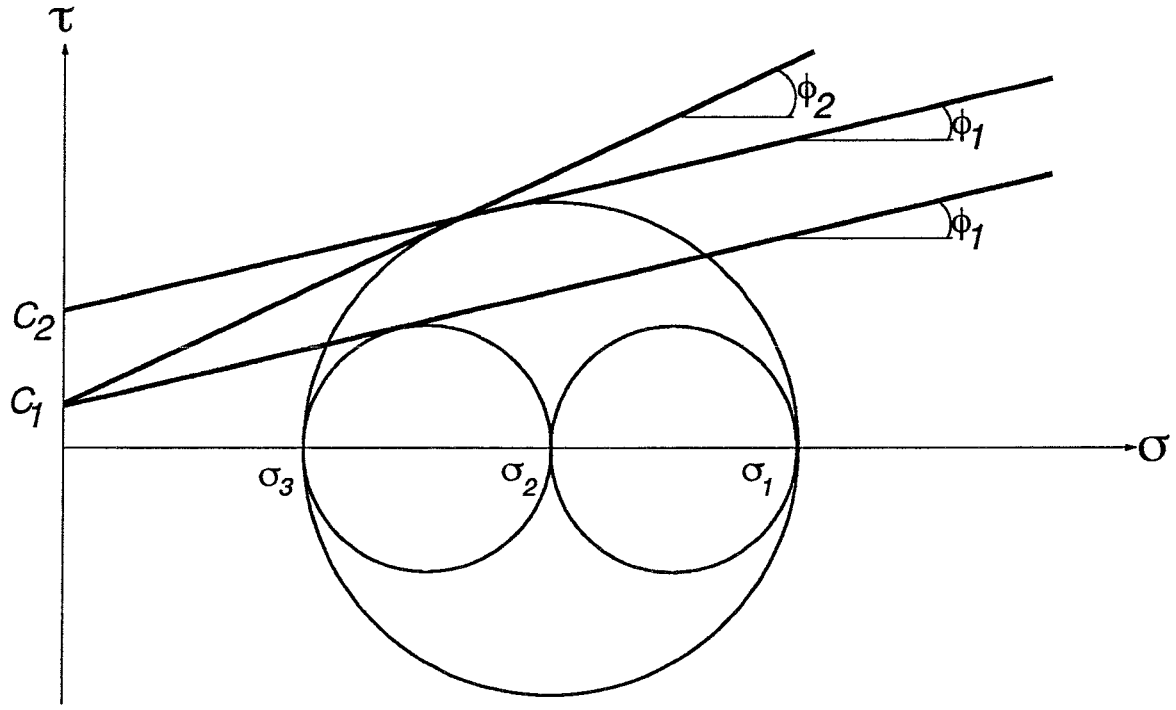

Figure 6.4 Principle description of strength requirements (i.e, cohesion and friction angle) to prevent shear failure, using σ_1-σ_3 and σ_2-σ_3 as maximum deviatoric stresses.

Notice that water flow in the fault zones was not simulated in this study. All results are based on steady-state assumptions. If, for instance, the pore pressure from the ice lake is prevented from decreasing when the ice sheet is retreating, a different displacement field is most likely to occur. For example, this situation can result from near surface permafrost.

7 CONCLUSIONS AND RECOMMENDATIONS

The following conclusions can be drawn based on this study;

1 The high in-situ stress state requires almost twice the fault zone friction angle of the low and the medium stress state to prevent failure of fault zones with in-situ stresses acting in the model. The high in-situ stress state also requires the highest fault zone cohesion of the stress state modelled in this study, as shown in Figure 7.1.

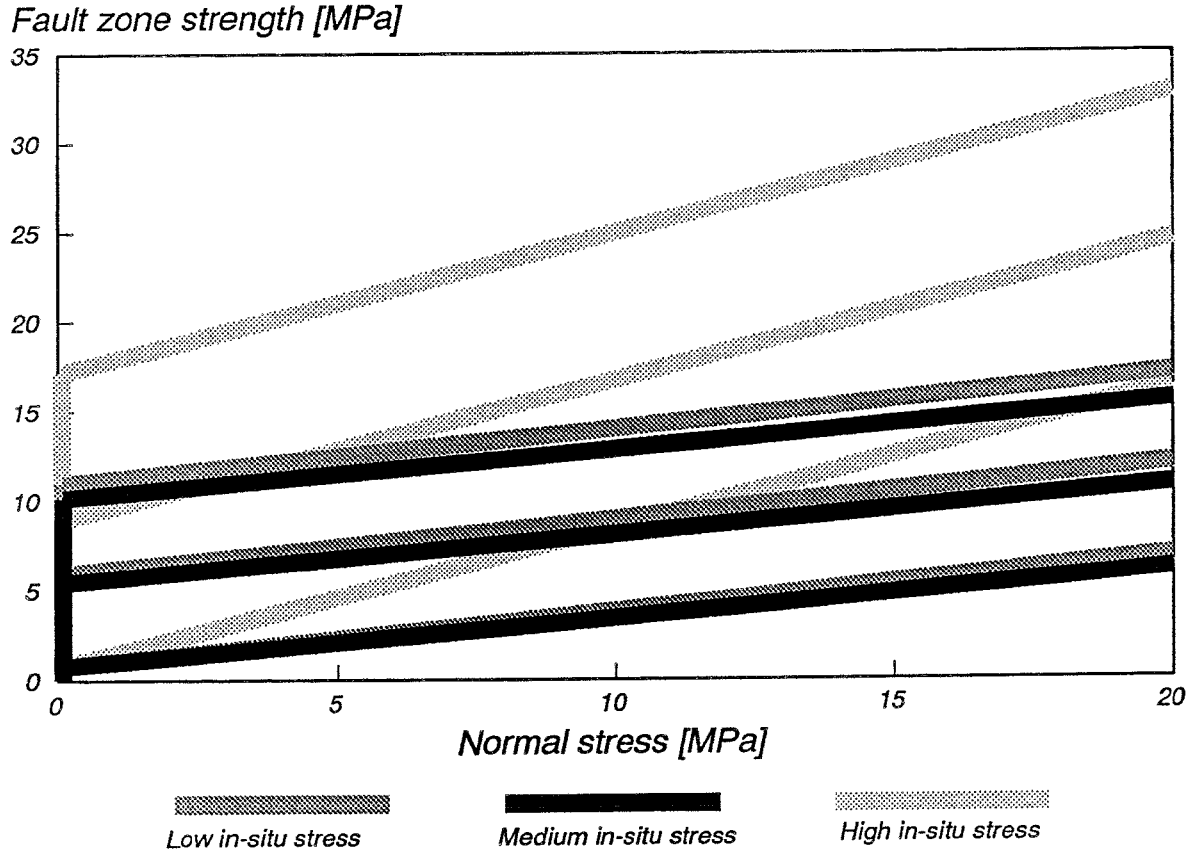

Figure 7.1 Fault zone failure envelopes for all combinations of Low, Medium and High in-situ stress state and Minimum, Mean and Maximum fault zone strength.

2 The low in-situ stress state shows significant reactions to the introduction of an ice lake with minimum and mean fault zone strength and, with an ice lake, to changes in fault zone strength.

3 The least reaction from the surface ice load and the pore pressure change can be seen in the analysis with the high in-situ stress.

4 The medium in-situ stress gives an hydrostatic stress condition at a depth of approximately 940 m. When the ice load of 3 km thickness is applied, the hydrostatic stress belt is transferred to approximately 300 m depth. The belt of infinite strength/stress ratio for fault zone failure, which the hydrostatic stress gives, will pass through the potential repository depth of 600-650 m,

recommended by Rosengren and Stephansson (1990), when the ice sheet is approximately 850 m thick.

5 All cases without the ice lake show stress anomalies in the vicinity of Fault Zones 2 and 14, regardless of stress state. The stress anomalies are caused by mostly elastic deformations of the fault zones from the ice sheet. The weight of the overlying ice is compensated or exceeded by the increased pore pressure from the ice lake. Therefore, the deformations in the two fault zones is diminished and therefore also the stress anomalies. The only exception from that can be seen for the low in-situ stress state, using the minimum and mean fault zone strength in which the stresses were reoriented locally; high stress concentrations were observed in connection with failed fault zones even for the ice lake cases.

6 The shear strength of the fault zones was a combination of a normal stress dependent portion via the friction angle, and a stress independent part via the cohesion. The reaction of the rock mass to pore pressure increase will differ depending on the combination of friction and cohesion. The more linear and flat the shear strength/stress curve, the greater length (depth) of the fault zone will be involved in a reduction of the shear strength/stress curve below F=1.

7 No effects on the stress distribution can be seen between the different strength cases except for the low in-situ stress models, which gives major stress disturbance in most of the models.

Based on this study, the following recommendations are given;

1) The recommendation by Rosengren and Stephansson, to locate a repository, between the Fault Zones 1, 5, 12 and 14 (see Figure 4.1) at a depth of 600-650 m, is valid in this study, as is the recommended width of the protection zone (100 m).

2) The finite loading condition results in a vertical displacement field that bends the model. The bending is likely to cause additional failure in the model. The effect of the bending can be studied by varying the width of a simple model (1-2 single fault zones). Also the depth of the model should be varied in order to investigate the severe failure in the low stress, minimum and mean fault zone strength cases. If the UDEC code was modified to handle loading of the boundary elements outside the distinct element domain, a detailed study of the influence of the ice sheet width and the displacement field could be conducted.

3) This study was performed using a two-dimensional model. The displacements along joints are believed to be overestimated in 2-d due to the assumed perpendicular strike of the joints. On the other hand, no account has been taken to the major horizontal principal in-situ stress σ_H. The effects of the increased deviatoric stresses from using σ_H instead of σ_h are difficult to estimate. A three-dimensional model using dip and dip direction of the fault zones and the complete 3-d in-situ stress will simulate the 3-d effects on the stress and displacement fields in a more rigorous manner. A 3-dimensional model will also give the opportunity to compare model results from different stress/strength assumptions to known geological events, such as observed shear directions along fault zones, type of failure and, to some extent magnitudes of displacements. This procedure is

promising as another method of calibration which can reduce the number of possible stress/strength combinations. The methodology used in this study, in defining in-situ stresses, fault zone strengths etc, is applicable to any site. Therefore, this type of study, initiated at an early stage, can indicate the suitability of a potential site.

4) To validate the assumptions of stress versus depth, an extension of the stress measurement profile from 502 m level down to 1000 m level is recommended.

8 ACKNOWLEDGEMENTS

The authors would like to extend their thanks to Dr. Loren Lorig of Itasca, Minneapolis, for his support and guidance during this project and to Magnus Liedholm of VBB/VIAK, Gothenburg, who conducted the statistical processing of stress data.

9 REFERENCES

Ahlbom, K. and Tirén, S. 1989. Overview of geologic and hydrogeologic character of the Finnsjön Site and its surroundings. Technical Report IRAP 89206, Swedish Geological, Uppsala.

Axelsson, K. 1983. Continuum mechanics. Division of Structural Engineering, Luleå University of Technology, Luleå. (In Swedish)

Bjarnason, B. and Stephansson, O. 1988. Hydraulic fracturing stress measurements in Borehole Fi-6 Finnsjön study site, Central Sweden. SKB Working Report R&D 88-54, Swedish Nuclear Fuel and Waste Management Company, Stockholm.

Björck, S. and Svensson, N-O. 1990. Climatic changes and uplift patterns - past, present and future. SKB Technical Report, In press.

Eronen, M. and Olander, H. 1990. On the World's ice ages and changing environments. University of Helsinki. Report YJT-90-13, Nuclear Waste Commission of Finnish Power Companies, Helsinki.

Itasca Consulting Group, Inc. 1991. UDEC, Version 1.7, Vol.I and II, User's manual and Verification and example problems.

Rosengren, L. and Stephansson, O. 1990. Distinct Element Modelling of The Rock Mass Response to Glaciation at Finnsjön, Central Sweden, SKB Technical Report 90-40.

Stephansson, O., Särkkä, P. and Myrvang, A. 1986. State of stress in Fennoscandia. In: O. Stephansson (Ed.) Proc. Int. Symp. on Rock Stress and Stress Measurements, Centek Publishers, Luleå, pp.21-32.

Swan, G., 1978. The Mechanical Properties of Stripa Granite, LBL-7074, SAC-03, Berkeley, California.

STATE OF STRESS AT AN ARBITRARY POINT OF AN INFINITE HALFSPACE OF ELASTIC MATERIAL SUBJECTED TO A TWO-DIMENSIONAL LOADING,Q

The equations used to obtain the stress induced from a two-dimensional loading, q, at an arbitrary point of an infinite half-space of elastic material, Figure 1, is;

$$\Delta\sigma_x=\frac{q}{2\pi}\left[2(\varphi 1-\varphi 2)-(sin2\varphi 1-sin2\varphi 2)\right] \quad (1)$$

$$\Delta\sigma_y=\frac{q}{2\pi}\left[2(\varphi 1-\varphi 2)+(sin2\varphi 1-sin2\varphi 2)\right] \quad (2)$$

where $\Delta\sigma_x$ and $\Delta\sigma_y$ is the induced horizontal and vertical stress components due to the loading, and 2a is the width of the strip load, q, see Figure 1. The total horizontal and vertical stress (i.e., $\sigma_x=\sigma_x^{in\text{-}situ}+\Delta\sigma_x$ & $\sigma_y=\sigma_y^{in\text{-}situ}+\Delta\sigma_y$) and the pore pressure is then used to calculate the effective normal and shear stress, acting on each fault zone in the model.

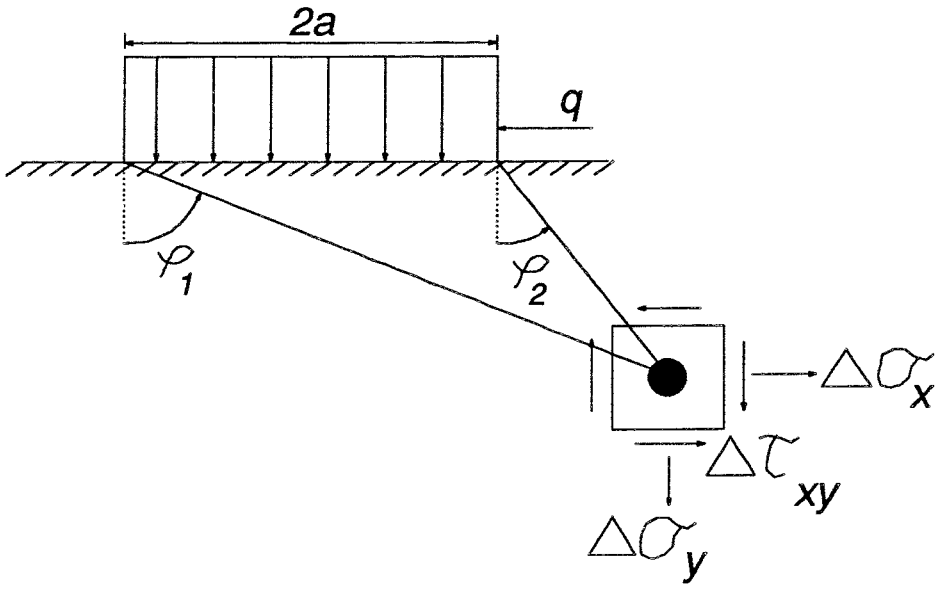

Figure 1 Induced state of stress at point of an infinite halfspace subjected to a finite uniformly distributed strip load, q.

The effective normal stress σ'_N is used to calculate the shear strength of the fault zone according to

$$\tau_{strength}=C+\sigma'_N*\tan\phi \quad (3)$$

where C = fault zone cohesion and ϕ = fault zone friction angle.

The shear strength/stress ratio is defined as

$$F=\frac{\tau_{strength}}{\tau_{actual}} \quad (4)$$

List of SKB reports

Annual Reports

1977-78
TR 121
KBS Technical Reports 1 – 120
Summaries
Stockholm, May 1979

1979
TR 79-28
The KBS Annual Report 1979
KBS Technical Reports 79-01 – 79-27
Summaries
Stockholm, March 1980

1980
TR 80-26
The KBS Annual Report 1980
KBS Technical Reports 80-01 – 80-25
Summaries
Stockholm, March 1981

1981
TR 81-17
The KBS Annual Report 1981
KBS Technical Reports 81-01 – 81-16
Summaries
Stockholm, April 1982

1982
TR 82-28
The KBS Annual Report 1982
KBS Technical Reports 82-01 – 82-27
Summaries
Stockholm, July 1983

1983
TR 83-77
The KBS Annual Report 1983
KBS Technical Reports 83-01 – 83-76
Summaries
Stockholm, June 1984

1984
TR 85-01
Annual Research and Development Report 1984
Including Summaries of Technical Reports Issued during 1984. (Technical Reports 84-01 – 84-19)
Stockholm, June 1985

1985
TR 85-20
Annual Research and Development Report 1985
Including Summaries of Technical Reports Issued during 1985. (Technical Reports 85-01 – 85-19)
Stockholm, May 1986

1986
TR 86-31
SKB Annual Report 1986
Including Summaries of Technical Reports Issued during 1986
Stockholm, May 1987

1987
TR 87-33
SKB Annual Report 1987
Including Summaries of Technical Reports Issued during 1987
Stockholm, May 1988

1988
TR 88-32
SKB Annual Report 1988
Including Summaries of Technical Reports Issued during 1988
Stockholm, May 1989

1989
TR 89-40
SKB Annual Report 1989
Including Summaries of Technical Reports Issued during 1989
Stockholm, May 1990

1990
TR 90-46
SKB Annual Report 1990
Including Summaries of Technical Reports Issued during 1990
Stockholm, May 1991

1991
TR 91-64
SKB Annual Report 1991
Including Summaries of Technical Reports Issued during 1991
Stockholm, April 1992

Technical Reports

List of SKB Technical Reports 1992

TR 92-01
GEOTAB. Overview
Ebbe Eriksson[1], Bertil Johansson[2], Margareta Gerlach[3], Stefan Magnusson[2], Ann-Chatrin Nilsson[4], Stefan Sehlstedt[3], Tomas Stark[1]
[1]SGAB, [2]ERGODATA AB, [3]MRM Konsult AB
[4]KTH
January 1992

TR 92-02
Sternö study site. Scope of activities and main results
Kaj Ahlbom[1], Jan-Erik Andersson[2], Rune Nordqvist[2], Christer Ljunggren[3], Sven Tirén[2], Clifford Voss[4]
[1]Conterra AB, [2]Geosigma AB, [3]Renco AB,
[4]U.S. Geological Survey
January 1992

TR 92-03
Numerical groundwater flow calculations at the Finnsjön study site – extended regional area
Björn Lindbom, Anders Boghammar
Kemakta Consultants Co, Stockholm
March 1992

TR 92-04
Low temperature creep of copper intended for nuclear waste containers
P J Henderson, J-O Österberg, B Ivarsson
Swedish Institute for Metals Research, Stockholm
March 1992

TR 92-05
Boyancy flow in fractured rock with a salt gradient in the groundwater – An initital study
Johan Claesson
Department of Building Physics, Lund University, Sweden
February 1992

TR 92-06
Characterization of nearfield rock – A basis for comparison of repository concepts
Roland Pusch, Harald Hökmark
Clay Technology AB and Lund University of Technology
December 1991

TR 92-07
Discrete fracture modelling of the Finnsjön rock mass: Phase 2
J E Geier, C-L Axelsson, L Hässler,
A Benabderrahmane
Golden Geosystem AB, Uppsala, Sweden
April 1992

TR 92-08
Statistical inference and comparison of stochastic models for the hydraulic conductivity at the Finnsjön site
Sven Norman
Starprog AB
April 1992

TR 92-09
Description of the transport mechanisms and pathways in the far field of a KBS-3 type repository
Mark Elert[1], Ivars Neretnieks[2], Nils Kjellbert[3], Anders Ström[3]
[1]Kemakta Konsult AB
[2]Royal Institute of Technology
[3]Swedish Nuclear Fuel and Waste Management Co
April 1992

TR 92-10
Description of groundwater chemical data in the SKB database GEOTAB prior to 1990
Sif Laurent[1], Stefan Magnusson[2], Ann-Chatrin Nilsson[3]
[1]IVL, Stockholm
[2]Ergodata AB, Göteborg
[3]Dept. of Inorg. Chemistry, KTH, Stockholm
April 1992

TR 92-11
Numerical groundwter flow calculations at the Finnsjön study site – the influence of the regional gradient
Björn Lindbom, Anders Boghammar
Kemakta Consultants Co., Stockholm, Sweden
April 1992

TR 92-12
HYDRASTAR – a code for stochastic simulation of groundwater flow
Sven Norman
Abraxas Konsult
May 1992

TR 92-13
Radionuclide solubilities to be used in SKB 91
Jordi Bruno[1], Patrik Sellin[2]
[1]MBT, Barcelona Spain
[2]SKB, Stockholm, Sweden
June 1992

TR 92-14
Numerical calculations on heterogeneity of groundwater flow
Sven Follin
Department of Land and Water Resources, Royal Institute of Technology
June 1992

TR 92-15
Kamlunge study site.
Scope of activities and main results
Kaj Ahlbom[1], Jan-Erik Andersson[2],
Peter Andersson[2], Thomas Ittner[2],
Christer Ljunggren[3], Sven Tirén[2]
[1]Conterra AB
[2]Geosigma AB
[3]Renco AB
May 1992

TR 92-16
Equipment for deployment of canisters with spent nuclear fuel and bentonite buffer in horisontal holes
Vesa Henttonen, Miko Suikki
JP-Engineering Oy, Raisio, Finland
June 1992

TR 92-17
The implication of fractal dimension in hydrogeology and rock mechanics Version 1.1
W Dershowitz[1], K Redus[1], P Wallmann[1],
P LaPointe[1], C-L Axelsson[2]
[1]Golder Associates Inc., Seattle, Washington, USA
[2]Golder Associates Geosystem AB, Uppsala, Sweden
February 1992

TR 92-18
Stochastic continuum simulation of mass arrival using a synthetic data set. The effect of hard and soft conditioning
Kung Chen Shan[1], Wen Xian Huan[1], Vladimir Cvetkovic[1], Anders Winberg[2]
[1] Royal Institute of Technology, Stockholm
[2] Conterra AB, Gothenburg
June 1992

TR 92-19
Partitioning and transmutation.
A review of the current state of the art
Mats Skålberg, Jan-Olov Liljenzin
Department of Nuclear Chemistry,
Chalmers University of Technology
October 1992

TR 92-20
SKB 91
Final disposal of spent nuclear fuel. Importance of the bedrock for safety
SKB
May 1992

TR 92-21
The Protogine Zone.
Geology and mobility during the last 1.5 Ga
Per-Gunnar Andréasson, Agnes Rodhe
September 1992

TR 92-22
Klipperås study site.
Scope of activities and main results
Kaj Ahlbom[1], Jan-Erik Andersson[2],
Peter Andersson[2], Tomas Ittner[2],
Christer Ljunggren[3], Sven Tirén[2]
[1]Conterra AB
[2]Geosigma AB
[3]Renco AB
September 1992

TR 92-23
Bedrock stability in Southeastern Sweden. Evidence from fracturing in the Ordovician limestones of Northern Öland
Alan Geoffrey Milnes[1], David G Gee[2]
[1]Geological and Environmental Assessments (GEA), Zürich, Switzerland
[2]Geologiska Institutionen, Lund, Sweden
September 1992

TR 92-24
Plan 92
Costs for management of the radioactive waste from nuclear power production
Swedish Nuclear Fuel and Waste Management Co
June 1992

TR 92-25
Gabbro as a host rock for a nuclear waste repository
Kaj Ahlbom[1], Bengt Leijon[1], Magnus Liedholm[2],
John Smellie[1]
[1]Conterra AB
[2]VBB VIAK
September 1992

TR 92-26
Copper canisters for nuclear high level waste disposal. Corrosion aspects
Lars Werme, Patrik Sellin, Nils Kjellbert
Swedish Nuclear Fuel and Waste Management Co, Stockholm, Sweden
October 1992

TR 92-27

Thermo-mechanical FE-analysis of butt-welding of a Cu-Fe canister for spent nuclear fuel

B L Josefson[1], L Karlsson[2], L-E Lindgren[2], M Jonsson[2]
[1]Chalmers University of Technology, Göteborg, Sweden
[2]Division of Computer Aided Design, Luleå University of Technology, Luleå, Sweden
October 1992

TR 92-28

A rock mechanics study of Fracture Zone 2 at the Finnsjön site

Bengt Leijon[1], Christer Ljunggren[2]
[1]Conterra AB
[2]Renco AB
January 1992

TR 92-29

Release calculations in a repository of the very long tunnel type

L Romero, L Moreno, I Neretnieks
Department of Chemical Engineering,
Royal Institute of Technology, Stockholm, Sweden
November 1992

TR 92-30

Interaction between rock, bentonite buffer and canister. FEM calculations of some mechanical effects on the canister in different disposal concepts

Lennart Börgesson
Clay Technology AB, Lund Sweden
July 1992

TR 92-31

The Äspö Hard Rock Laboratory: Final evaluation of the hydrogeochemical pre-investigations in relation to existing geologic and hydraulic conditions

John Smellie[1], Marcus Laaksoharju[2]
[1]Conterra AB, Uppsala, Sweden
[2]GeoPoint AB, Stockholm, Sweden
November 1992

TR 92-32

Äspö Hard Rock Laboratory. Evaluation of the combined longterm pumping and tracer test (LPT2) in borehole KAS06

Ingvar Rhén[1] (ed.), Urban Svensson[2] (ed.), Jan-Erik Andersson[3], Peter Andersson[3], Carl-Olof Eriksson[3], Erik Gustafsson[3], Thomas Ittner[3], Rune Nordqvist[3]
[1]VBB VIAK AB
[2]Computer-aided Fluid Engineering
[3]Geosigma AB
November 1992

TR 92-33

Finnsjö Study site. Scope of activities and main results

Kaj Ahlbom[1], Jan-Erik Andersson[2], Peter Andersson[2], Thomas Ittner[2], Christer Ljunggren[3], Sven Tirén[2]
[1]Conterra AB
[2]Geosigma AB
[3]Renco AB
December 1992